

LASER-INDUCED GROWTH OF NANOPARTICLES AND NANOSTRUCTURES

By

Leonardo C. Pacheco-Londoño

A dissertation submitted in partial fulfillment of the requirements for the degree of

DOCTOR OF PHILOSOPHY
in
Applied Chemistry

UNIVERSITY OF PUERTO RICO
MAYAGÜEZ CAMPUS
2011

Approved by:

Nairmen Mina-Camilde, Ph.D.
Member, Graduate Committee

Date

Félix E. Fernández, Ph.D.
Member, Graduate Committee

Date

Fernando A. Souto-Bachiller, Ph.D.
Member, Graduate Committee

Date

Marco A. De Jesús, Ph.D.
Member, Graduate Committee

Date

Julio G. Briano-Peralta, Ph.D.
Member, Graduate Committee

Date

Samuel P. Hernandez-Rivera, PhD
President, Graduate Committee

Date

Narinder K Mehta, Ph.D.
Representative of Graduate Studies

Date

Francis Patron, Ph.D.
Chairperson of the Department

Date

Abstract is Presented to the Graduate School
of the University of Puerto Rico in Partial Fulfillment of the
Requirements for the Degree of DOCTOR OF PHILOSOPHY

**LASER-INDUCED GROWTH OF NANOPARTICLES AND
NANOSTRUCTURES**

By

Leonardo C. Pacheco-Londoño

2011

Chair: Samuel P. Hernandez-Rivera
Major Department: Chemistry

The preparation of nanostructures assisted by laser action was studied and successfully accomplished from solution and on surfaces. The synthesized nanostructures were characterized by several microscopy techniques. Silver, gold, copper and platinum nanoparticles were grown on surfaces in the form of patterns by the exposure of laser radiation onto droplets of metal ion solutions and the aid of a reducing agent. The generation of patterns from metallic nanoparticles (NPs) was achieved by combining induced growth of nanoparticles and nanostructures by laser incidence directly on surfaces (LIDS) and optical image formation techniques for transferring the patterns. Near-ultraviolet (363.8 nm) and visible (532 nm) laser wavelengths were used for the laser induced growth of NPs into microstructures on glass, quartz, stainless steel, silicon and gold-on-silicon substrates. The sizes of the patterns formed were on the micrometer scale and the sizes of the transferred patterns were on the millimeter scale. The patterns formed were generated by optical transference of image and interference of laser beams. Ag and Au substrates were highly active in surface enhanced Raman spectroscopy (SERS). The enhanced Raman activity was measured for SERS probe molecules: 9H-purin-6-amine (adenine) and 1,2-bis(4-pyridyl)-ethane (BPE)

analytes on Ag and Au substrates, respectively. The enhancement factor obtained were 1.8×10^5 and 6.2×10^6 respectively. The growth Ag nanoparticles in solution and their conversion to nanoprisms induced by laser radiation action were studied and the kinetics of growth and conversion processes was measured. A mechanism for the growth and conversion from nanoparticle seeds to nanostructures consisting of two processes was proposed. The kinetics for the two processes was measured and the dependence of rate of growth and conversion with laser power was obtained. The quantum efficiency for the processes was also measured. The first process consisting of agglomeration was found to depend on the probability of excitation of plasmon the initial nanoparticles (seeds). This first process is necessary for the second process (growth process) to occur and controls it in an indirect way. Nucleation and crystallization of nanoprisms and the growth of crystal are produced by the NP excited by light. The size of the crystals obtained is controlled by the wavelength of the incident light in the second process. The growth begins by an agglomeration process followed by fusion of the nanoparticles to produce small crystals and finally the growth of relatively large crystals. SERS activity was measured for three different analytes, several types of nanoprisms and various Raman excitation lines. Enhanced Raman activity was measured for nanoprisms in aqueous suspensions and on surfaces. The activity SERS for the nanoprisms is better when those are on substrate surfaces. It is possible have a considerable repeatability when a gold surface is treated with a solution of S^{2-} anions.

Resumen es Presentado a Escuela Graduada
de la Universidad de Puerto Rico como requisito parcial de los
Requerimientos para el grado de DOCTOR EN FILOSOFIA

**CRECIMIENTO OF NANOPARTICULAS Y NANOESCTRUTURAS
USANDO LASER**

Por

Leonardo C. Pacheco-Londoño

2011

Consejero: Samuel P. Hernandez-Rivera
Departamento: Quimica

La preparación de nanoestructuras asistida por acción de láseres se estudió y fue exitosamente llevada a cabo en solución y sobre superficies. Las nanoestructuras sintetizadas fueron caracterizadas fue realizada por varias técnicas de microscopía. Nanopartículas de plata, oro, cobre y platino fueron sintetizadas sobre superficies por exposición de la radiación láser sobre una gotita de solución de iones metálicos y un agente reductor. Laser de ultravioleta cercano (363.8 nm) y visible (532 nm) se utilizaron para el crecimiento inducido de las nanopartículas sobre vidrio, cuarzo, acero inoxidable y sobre silicio cubierto de oro. Los tamaños de los patrones formados fueron de escala de micrómetros y los tamaños de los patrones transferidos eran en la escala de milímetros. El tamaño de los patrones obtenidos está limitado por la longitud de onda de la luz, el tamaño del objeto que acta como la imagen del patrón para generar la imagen transferida y el diseño de ópticas empleadas. La falta de nitidez cuando la imagen del patrón es ópticamente transferido está limitada por la configuración óptica debido a que el proceso de deposición es al azar en el sitio irradiado. Un efecto de penumbra también puede inducir el crecimiento de nanopartículas en los alrededores de la imagen, disminuyendo la nitidez de la imagen en las fronteras. Los

substratos de Ag y Au fueron activos para espectroscopia Raman aumentada sobre superficie. La actividad fue medida para 9H-purina-6 amina (adenina) y 1,2-bis(4-piridil)-etano (BPE) como analitos sobre los substratos de Ag y Au respectivamente. El factor de aumento fue 1.8×10^5 y 6.2×10^6 respectivamente. El crecimiento de nanopartículas de Ag en solución y su conversión a nanoprismas inducidos por acción de radiación láser se estudió y la cinética de los procesos de crecimiento y conversión se midió. Un mecanismo para el crecimiento y conversión de semillas de nanopartículas a nanoestructuras se propuso. La cinética de los dos procesos se midió y la dependencia de la rapidez de crecimiento con la potencia del láser se obtuvo. La eficiencia cuántica para los procesos también se midió. El primer proceso consistente de aglomeración se encontró que tiene una dependencia en la probabilidad de la excitación de las oscilaciones colectivas de electrones de en la banda de conducción del metal o plasmón de las nanopartículas iniciales (semillas) utilizadas para el crecimiento inducido por radiación láser. Este primer proceso es necesario para que se de paso al segundo proceso (de conversión) y controla el mismo en forma indirecta. La nucleación y cristalización de nanoprismas y el crecimiento cristalino se producen mediante la excitación de las nanopartículas por luz. El tamaño de los cristales obtenidos se controla con la longitud de onda de la luz incidente en el segundo proceso. El crecimiento comienza con un proceso de aglomeración seguido por la fusión de nanopartículas para producir pequeños cristales y finalmente crecimiento de cristales relativamente grandes. Actividad SERS se midió para tres analitos diferentes, varios tipos de nanoprimas y varias longitudes de onda de excitación Raman. Actividad Raman realizada por superficies se midió para nanoprismas en suspensiones acuosas y en superficies de sustratos. La actividad SERS de los nanoprismas fue mayor cuando las nanoestructuras se depositaron sobre superficies y se enlazaron fuertemente al sustrato de oro. Se demostró que es posible conseguir buena reproducibilidad cuando se utiliza una superficie de oro tratada con una solución de aniones S^{2-} .

Copyright © 2011

by

Leonardo C. Pacheco-Londoño

To my family, lili and my son in heaven . .

ACKNOWLEDGMENTS

I want to start expressing a sincere acknowledgement to my advisor, Dr. Samuel P. Hernández for his advice.

I also want to express my sincere acknowledgement to the members of my graduate committee and all my professors that contributed to my education of the departments of Chemistry, Physics and Engineering of University of Puerto Rico, Mayaguez Campus .

Thanks to Oliva Primera, William Ortiz, Eduardo Espinosa, John Castro, Jose L Ruiz, Michael Ramirez, Hilsamar Félix, Sandra Correa and Jorge Guette for their friendship.

Parts of the work presented in this contribution were supported by the U.S. Department of Defense, University Research Initiative Multidisciplinary University Research Initiative (URI)-MURI Program, under grant number DAAD19-02-1-0257.

Support from the U.S. Department of Homeland Security under Award Number 2008-ST-061-ED0001 is also acknowledged. However, the views and conclusions contained in this document are those of the authors and should not be interpreted as necessarily representing the official policies, either expressed or implied, of the U.S. Department of Homeland Security.

TABLE OF CONTENTS

	<u>page</u>
ABSTRACT ENGLISH	ii
ABSTRACT SPANISH	iv
ACKNOWLEDGMENTS	viii
LIST OF TABLES	xi
LIST OF FIGURES	xii
LIST OF ABBREVIATIONS	xiii
LIST OF SYMBOLS	xiv
1 INTRODUCTION	1
1.1 General Aspects	1
1.2 Previous work	3
2 GROWTH OF AG, AU, CU, AND PT NANOSTRUCTURES ON SURFACES BY MICROPATTERNED LASER IMAGE FORMATIONS	5
2.1 Methodology and experimental setup	5
2.1.1 Materials	5
2.1.2 Surface Cleanliness and preparation	5
2.1.3 Preparation of the Growth Solution	6
2.1.4 Growth Induction of Nanoparticles	6
2.1.5 Experimental Setup	7
2.1.6 Raman Experiment	9
2.2 Results	9
3 KINETICS OF LASER-INDUCED GROWTH OF SILVER NANOPRISMS	17
3.1 Methodology and experimental setup	17
3.1.1 Materials	17
3.1.2 Seed NPs form growth solution	17
3.2 Experimental Setup	18
3.2.1 Kinetics of conversion to nanoprisms	18
3.2.2 Raman Experiment	18
3.3 Results	19
3.3.1 Induction with different wavelengths	19

3.3.2	Growth induction using wavelengths shorter than 400 nm	19
3.3.3	Induction of growth using wavelengths longer than 400 nm	20
4	SURFACE ENHANCED RAMAN SCATTERING	29
4.1	SERS Activity for the micropattern	29
4.2	SERS dependence on induction of nanoprism with different wavelengths .	30
4.3	SERS activity of nanoprisms on surface	32
5	CONCLUSION	37
	APPENDICES	40
A	BACKGROUND INFORMATION	41
A.1	Nature of Light	41
A.2	Crystallization	41
A.3	Diffusion theory of crystallization	42
A.4	Surface Enhanced Raman Scattering	42

LIST OF TABLES

<u>Table</u>		<u>page</u>
2-1	Minimum exposure times (approximate values) for induced growth of NPs using LIDS with LIP on different substrates	11
2-2	Roughness indication parameters for AFM images	14
3-1	Rate constant for the agglomeration process for different laser powers and wavelengths	21
3-2	Quantum efficiency and coefficients of extinction for different wavelengths . .	22

LIST OF FIGURES

<u>Figure</u>	<u>page</u>
2-1 Optical setups used	8
2-2 White light images obtained by optical microscopy	15
2-3 TEM and AFM images for TPI	16
3-1 Setup for induction of conversion of nanospheres to nanoprisms	18
3-2 UV-Vis absorbance spectrum of Ag NPs seeds and their TEM images	20
3-3 Laser assisted growth induction of NPs using UV light and TEM images of nanostructures produced	24
3-4 UV/VIS spectra at different induction times	25
3-5 Kinetics of induction at different laser powers for the first process	26
3-6 Kinetics of induction at different laser powers for the second process	27
3-7 TEM image of crystallization process	28
4-1 Depths of TPI, SERS spectra for TPI and lineal maps of SERS activity	34
4-2 SERS activity of nanoprisms in solution	35
4-3 SERS activity of nanoprisms on Gold surface	36

LIST OF ABBREVIATIONS

NPs	Metallic nanoparticles
SERS	surface enhanced Raman spectroscopy
UHP	deionized ultra-high-purity
BPE	1,2-bis(4-pyridyl)-ethane
adenine	9H-purin-6-amine
EF	enhancement factor
LIDS	laser incidence directly on surfaces
PI	pattern image
ILB	interference of laser beams
LIP	linear interference pattern
TPIs	transferred pattern images
HR-TEM	high resolution transmission electron microscope
SEM	scanning electron microscope
AFM	atomic force microscope
NUV	near UV
OC	opposite contrast
EC	equal contrast
E°	standard reduction potential
ET	exposure time
RMS-R	root-mean-square roughness
PV-R	peak-to-valley roughness
A-R	average roughness

LIST OF SYMBOLS

t	Time (seconds)
cm^{-1}	wavenumber
μg	Micrograms
ng	Nanograms
pg	Picograms
fg	femtograms
λ	Wavelength
W	Watt (j/s)

CHAPTER 1

INTRODUCTION

1.1 General Aspects

Metallic nanoparticles (NPs) of various sizes and shapes can be synthesized from liquid solutions of metal ions by adding a reducing agent at relatively high temperatures (at the solvent boiling point) [1, 2] and by laser-induced reduction [3]. Optical properties of NPs prepared depend on the size and shape of the particles. The rate of formation of nanostructures, including nanoprisms depends on the wavelength of the incident photons used for the conversion and on the laser power of the light source. Synthesized NPs can also be attached to surfaces, resulting in substrates that can be used in a variety of applications. There are two well-established methods for constructing such substrates: electron beam lithography [4] and nanosphere lithography [5]. An alternative method consists of the induced growth of NPs by laser incidence directly on surfaces (LIDS) [6] or by the incidence of laser on a surface immersed in a solution [3, 7]. Parts of this investigation were based on the growth of NPs using LIDS on droplets of metallic ions solutions and the initial assistance of a reducing agent to produce a pattern image (PI) on the micrometer scale and synthesis of nanoprisms in solution from small nanoparticles of Ag by laser action, also use these as substrates for detection of trace analytes by SERS. The formation of the PI was accomplished using three optical arrangements:

1. setup 1 used a one-lens optical layout
2. setup 2 used a two-lens optical layout (applying the limits of the thin lens and paraxial approximations in both cases)
3. setup 3 used interference of laser beams (ILB) optical fronts by means of 50% beam

splitters to separate the optical fronts of the laser beams and then later recombining them at the substrate surface.

Diffraction phenomena allow the construction of PIs with either a one- or two-lens setup, according to Abbe's theory of image formation. In the case of ILB, two or more polarized and coherent laser beams converge on a specific site of a surface, on which the interference pattern is formed [8]. If the intensity of the beams is sufficiently high, well-delimited structures are formed by the interference pattern. This has been well documented in the literature [9–14]. The characteristics of the patterns reported in the literature have shown periodicity from 100 nm [15] to 50 μm [13], depending on the wavelength of the lasers and the angle between the beams. The depths obtained were between 5 and 500 nm, depending on laser exposure time, laser power and the number of pulses for intermittent laser sources (pulsed lasers) [15]. Multiple, simultaneous analyses based on Raman spectroscopy and particularly on Surface Enhanced Raman Spectroscopy (SERS) mediated by metallic NPs can be based on such pattern formations. These applications are important for improving process efficiency and analysis throughput because the regularity of the multiple microstructure grids that can be prepared using LIDS or ILB on NPs allows for multiplexing and parallelizing such analyses. Another application arises from the increasing interest of noble-metal NPs for optical and catalytic properties. Based on this trend, if the exposure time is sufficiently large and the laser power is relatively high, then the pattern is not composed of NPs but of a metal pattern at a higher scale, which is an important application for electronic circuits. A similar form of printed metal patterns using parallel laser printing on Ag thin films was reported by Shin et al. [16], which has applications in electronic transistors. Patterns prepared from metal structures may be useful in surface-plasmonic applications, such as design of diffractive optical elements and in optical communications [17]. Balan et al. [18] recently reported patterns generated from holographic recording with polymer-containing Ag-NPs used as diffraction gratings. This contribution has been intended to establish the grounds for preparing metallic NPs arrays in a ordered way on substrates so as to form patterns

or grids in a short time and affordable cost. As a typical application, SERS activity was demonstrated using some of the prepared transferred pattern images (TPIs).

It is possible to convert silver nanospheres to nanoprisms using photons [19] of wavelengths larger than the maximum of plasmon resonance absorption in the visible (VIS) region of silver nanospheres (398 nm for NPs of diameters of 1-10 nm) and tune their size and characteristic dimensions with the wavelengths of photons [17]. For the synthesis of nanoprisms a mechanism for the conversion and measurement of the rate at different wavelengths and laser powers is proposed. The suggested mechanism has two principal steps. First, a quick agglomeration process of seeds NPs. The rate for this step depends on laser power and coefficient of extinction of seeds NPs. Second, a growth process step for formation of nanoprisms which is controlled by the wavelength of the incident photons triggering the conversion. The formation of nanostructures from seeds has been envisioned as a three steps process: induction, growth and termination [19]. In the first step, the nanoseeds are transformed by induction. In the growth step nanoparticles are rearranged forming spherical nanoseeds occur during this stage [7]. The termination step is determined by symmetry and stability. The SERS activity is measure and its dependence on the plasmon excitation is tested, also the nanoprisms are placed on a gold surface and the SERS activity is measured too. In order to facilitate the adhesion of the nanoprisms to substrates, these were deposited on a gold surface pretreated with S^{2-} ions. It is possible to observe a larger dispersion of the nanoprisms on the surface treated with S^{2-} . SERS activity was measured and compared for surfaces treated and non treated with S^{2-} ions and the repeatability for the treated surface was better than no treated.

1.2 Previous work

Laser-induced growth and deposition of gold and silver NPs was done and used for preparing surface-enhanced Raman scattering substrates by Bjerneld et al. [6, 20]. NPs were grown on glass surfaces of a capillary tube in contact with an aqueous solution of metal

ions, a reducing agent and an analyte. SERS signals were measured in concert with the deposition process of NPs on surface of the capillary tubes in order to monitor of synthesis. Rhodamine 6G was used as analyte. The deposited gold on the glass surface was rough on the nanometer scale which made it ideal for obtaining SERS phenomenon.

Metal structures in the form of ordered patterns generate new perspectives to classical optical designs for diffraction [17]. Balan et al. [18] developed periodical ordered metal structures using silver NPs in an acrylic polymeric matrix. The NPs were synthesized by photoreduction and the patterns were generated by interference of laser beams (ILB). The wavelength of the laser used was 532 nm. They had an efficient approach to generate a micro optical element using this methodology. However, this is dependent on the efficiency of the coupling between the reaction used to generate the NPs and the photocurrent of the polymeric matrix.

Monochromatic light of different laser wavelengths can be used for production of monodispersed silver nanoparticles as demonstrated by Zheng et al. [7, 19]. They were able to synthesize monodisperse nanoprisms from Ag NPs seed by laser induced photo conversion. By monitoring the absorption spectrum during photo conversion, they found an increase in the particle sizes and new plasmonic component band in the visible absorption spectrum. They tried to give an explanation of the conversion process with simple observations of the absorption spectra and TEM images.

CHAPTER 2

GROWTH OF AG, AU, CU, AND PT NANOSTRUCTURES ON SURFACES BY MICROPATTERNED LASER IMAGE FORMATIONS

2.1 Methodology and experimental setup

2.1.1 Materials

Hydrogen tetrachloroaurate (III) hydrate ($\text{HAuCl}_4 \cdot 3\text{H}_2\text{O}$, 99.9985% Au; 49% Au, Puratrem) and silver nitrate (AgNO_3 , 99.9995%-Ag, Puratrem) were purchased from Strem Chemicals. Sodium citrate dihydrate (99%), PtCl_4 (99%), CuSO_4 (99%) and 1,2-bis-(4-pyridyl)-ethane (BPE; 99%) were acquired from Sigma-Aldrich Chemical Co. (Milwaukee, WI); Hydrazine (99%) was purchased from Thermo-Fisher Scientific International (Pittsburgh, PA) and 9H-purin-6-amine (adenine; 99.9%) was obtained from ICN Biomedicals (Aurora, OH). The laser systems employed for LIDS experiments were a 532 nm frequency-doubled solid-state diode Nd:YAG laser (Verdi, 6W, Coherent, Inc. Laser Group, Santa Clara, CA); 363.8 nm laser from an Innova-25/8 Sabre laser system (Coherent Inc.) and 785 nm laser system (diode laser system, Process Instruments, Inc., Salt Lake City, UT).

2.1.2 Surface Cleanliness and preparation

Glass and quartz substrates (1 cm x 1 cm) were first washed with AlconoxTM Lab detergent (White Plains, NY) and with Micro-90 Cleaning Solution (Cole-Parmer, Vernon Hills, IL). The surfaces were further cleaned with a piranha solution ($\text{H}_2\text{SO}_4/\text{H}_2\text{O}_2$; 3:1)

treatment. The surfaces were then rinsed with absolute ethanol and further rinsed with distilled and deionized ultra-high-purity (UHP) water. They were then allowed to dry under an ultra-high-purity nitrogen atmosphere. For the induction of Au NP on glass the front surfaces was coated with Cr. The glass surface was metallized under vacuum (1.0×10^{-6} Torr), in an electrothermal evaporator (Edwards Auto 306, Edwards Vacuum, Tewksbury, MA) The thickness of Cr deposited was 15 nm at 1 angstrom/s and was measured using a quartz microbalance.

2.1.3 Preparation of the Growth Solution

Solutions of 0.01 M AgNO_3 , PtCl_4 , CuSO_4 and HAuCl_4 were prepared in UHP water. Reducing agent solutions of 0.05 M citrate and 0.005 M hydrazine were also prepared. The metal ions and reducing agent solutions were mixed to produce the growth solution for aqueous Ag, Cu, Pt or Au ions required to synthesize the desired NPs (when the hydrazine was used the solutions were maintained at 0 °C). For visible laser induction growth of Au-NPs 0.01 M HAuCl_4 solutions were used. For UV laser induction growth of Au-NPs with source 1mM solutions of HAuCl_4 were required.

2.1.4 Growth Induction of Nanoparticles

A droplet of growth solution was transferred onto the test surface using micropipettes with sub-microliter capabilities. The substrate was placed in the target position under 532 nm or 363.8 nm laser irradiation with exposures times that ranged from 1 to 500 s at laser powers of 0.1-5.0 W, depending on the surface. Initially, the laser beam passed through the optical setup for the generation of a PI and was then guided to a direct contact on NPs droplets the growth induction process. This procedure was repeated by varying the radiation exposure time (ET) and laser power on the various substrates tested. After laser irradiation, the substrates were washed with UHP water and allowed to air-dry in an optics cabinet under controlled temperature and relative humidity.

2.1.5 Experimental Setup

Three different setups were used to generate the PIs and to transfer the image to the substrates. In the first setup, illustrated in Fig. 2-1(a), one lens was used for generating an inverted image of a symmetrical grid of $100 \times 100 \mu\text{m}$. It is possible to reduce or amplify the image dimensions by adjusting the distance d_0 (object distance) or d_i (image distance), fulfilling the thin-lens equation in the paraxial approximation [21].

$$\frac{1}{f} = \frac{1}{d_0} + \frac{1}{d_i} \quad (2.1)$$

In setup 2 (Fig. 2-1(b)), an inverted image of equal size was generated. Setup 3, shown in Fig. 2-1(c), was used for generating a one-dimensional pattern. When two polarized and coherent beams overlap, a one-dimensional (1-D) interference pattern is generated. These patterns have a defined geometry that depends on the wavelength of the laser beams and the angle between them. The intensity distribution for two beams is represented by equation:

$$I(x) = 2I_0 \left[\cos \left[\frac{4x\pi}{\lambda} \sin \left[\frac{\theta}{2} \right] \right] \right] \quad (2.2)$$

where I_0 is the intensity of one laser beam, λ is the laser wavelength, and θ is the angle between the two incident beams. The periodicity of the pattern can be calculated by equation:

$$d = \frac{\lambda}{2 \sin \left[\frac{\theta}{2} \right]} \quad (2.3)$$

If three beams are used, a two-dimensional (2-D) interference dot pattern is formed. When four beams are employed, a planar interference pattern is produced. A line pattern with thinner and higher peaks and thicker area between peaks is observed in comparison with that for two interfering beams [9].

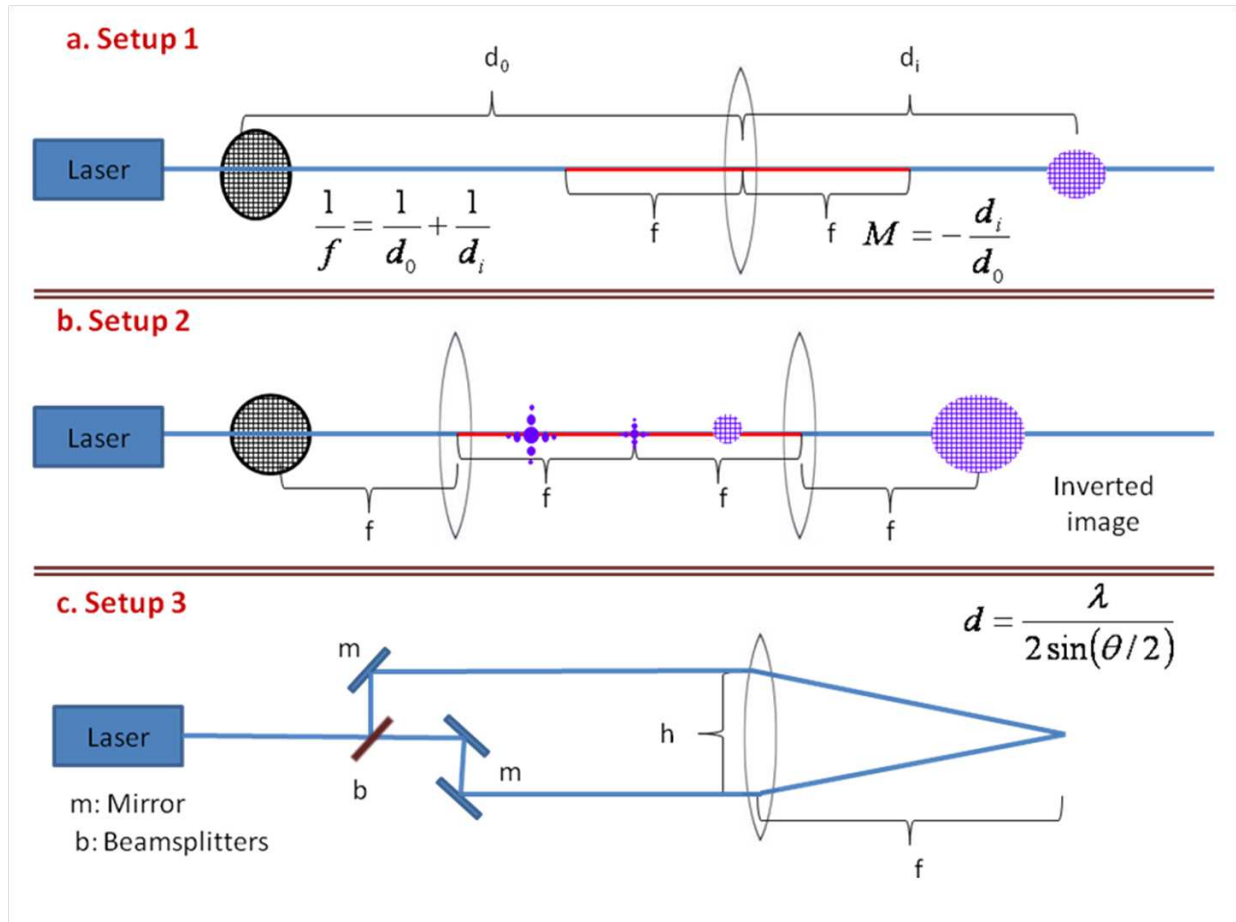


Figure 2–1: Optical setups used:(a) Setup 1: one-lens optical layout. (b) Setup 2: two-lens optical layout. (c) Setup 3: use of beam splitters. The object to lens distance is represented by d_0 ; d_i represents the image to lens distance; M is the transversal magnification; f focal length of the lens; b is the beamsplitter; m is a mirror; h is the lateral distance between the laser beams

The substrate surfaces produced and NPs used to prepare them were characterized by a high resolution transmission electron microscope (HR-TEM), Zeiss model 922 operated at 200 kV, by a scanning electron microscope (SEM) model JSM 6500 (JEOL-USA, Peabody, MA) and by an atomic force microscope (AFM) model CP-II (Veeco Instruments, Inc., Plainview, NJ). SEM images were obtained to characterize substrate surfaces and nanostructures formed on glass coated with gold. The AFM system was used for obtaining image information of nanostructures on glass.

2.1.6 Raman Experiment

Raman measurements were conducted using a RM2000 Renishaw Raman microspectrometer equipped with a Leica microscope (5× , 10× , 20× and 50× objectives). The spectra were collected in the Raman shift region of 200-3200 cm^{-1} (0.5 cm^{-1} resolution), with an integration time of 10 s. SERS enhancement factors (EF) were calculated for analytes on substrates according to the equation:

$$EF = \frac{I_{surf}}{I_{bulk}} \times \frac{N_{bulk}}{N_{surf}} \quad (2.4)$$

Where I_{surf} and I_{bulk} denote the intensity of a band of the analyte adsorbed on surface and the analyte in bulk, respectively. N_{surf} and N_{bulk} are the number of analyte molecule excited by the laser beam.

2.2 Results

Aluminum grids were used as a PI for setups 1 and 2, as shown in Fig. 2-1(a) and Fig. 2-1(b). The square grids, which were reflective at the UV and visible laser lines used, had an area of 100 x 100 μm^2 and the transparent edge had a width of 46 μm (see Fig. 2-2(a)). The PI in Fig. 2-2(b) is inverted but has an identical appearance due to the symmetry arising from the fact that the square grids were used as objects. TPIs of Ag-NPs were contracted by using setup 2 with a focus lens of 10 cm. A near UV (NUV) laser operating at 363.8 nm with intensity of 6.8 W/cm^2 was used for the formation of PIs and to transfer them on glass as TPIs. The nanostructures obtained were grouted on the edges. TPIs obtained using Pt- and Cu-NPs are shown in Fig. 2-2(c) and Fig. 2-2(d), respectively. These were generated using setup 1 with a 10 cm focal length lens, $d_0 = d_i = 20$ cm and the NUV laser line at 363.8 nm with an intensity of 1.7 W/cm^2 . Similar TPIs were obtained using setup 2. Fig. 2-2(e) shows a reduced TPI fabricated by setup 1 using Ag-NPs with 532 nm laser line using at an intensity of 2.3 kW/cm^2 . The reduced TPI was generated using a 2 cm focal length lens, a d_0 of 70 cm, and d_i of 2 cm. The transferred image is inverted and the deposition of NPs occurred with opposite contrast

(OC) with respect of that of the PI. Fig. 2-2(f) shows the case for $d_0 = f = 10$ cm and $d_i = 12$ cm. The TPI produced had equal contrast (EC) with respect to that of the PI. At $d_0 = f = 10$ cm and $d_i = 15$ cm, the TPI formed showed OC with respect to the PI, as shown in Fig. 2-2(g). According to the previous results, the induction carried out at different distances from the lens exhibited contrast variation and size increase, which can be exploited for various applications. One of the TPIs made from Au-NPs is shown in Fig. 2-2(h). This TPI was obtained using setup 1 with a 10 cm focal length lens ($d_0 = 20$ cm; $d_i = 20$ cm) and a laser intensity of 6.7 W/cm^2 at 363.8 nm and an ET of 300 s on Si. Using the same experimental conditions TPIs made from Au-NPs on glass and on glass coated with 15 nm Cr are illustrated in Fig. 2-2(i) and Fig. 2-2(j), respectively. The TPI using glass with 15 nm of Cr was made by depositing Au-NPs for an ET of only 120 s. The Au is photoreduced on surface but the process is faster on the glass surface metallized with 15 nm Cr. This is because the Cr assists in the reduction of $\text{AuCl}_4^-(\text{aq})$ ion to Au(s). The participation of Cr in the reduction process of Au makes the process faster and more efficient. The standard reduction potential (E°) for $\text{AuCl}_4^-(\text{aq})$ ion to Au(s) is 1.002 V and the Cr^{+3} to Cr is -0.74 V. The E° for the reaction is 1.742 V, which indicates that the reduction is thermodynamically spontaneous. However, if the glass substrate with Cr is submerged into a solution 1 mM of $\text{AuCl}_4^-(\text{aq})$ ions after 24 hours a layer of Au is formed on the coating Cr on the glass substrate, demonstrating that the reaction proceeds even without laser irradiation assistance. The adhesion of these metals on glass is in general quite weak. The NPs deposited can be removed by ultrasonic treatment. Substrates of Ag- or Au-NPs on glass (such as the ones shown in Fig. 2-2(e) to Fig. 2-2(i)) are removed completely in 45 min of ultrasonic treatment. However, when the deposition of Au was made on Cr coated glass it was not possible to remove the deposited NPs by ultrasonic treatment. The TPI shown in Fig. 2-2(j) could only be removed by mechanical abrasion. The time required to obtain NPs in the induction process depended on the wavelength of the laser (363.8 nm or 532 nm), the laser intensity and type of substrates used. However,

Table 2–1: Minimum exposure times (approximate values) for induced growth of NPs using LIDS with LIP on different substrates

Substrate	Ag 532.0nm	Ag 363.8nm	Pt 363.8nm	Cu 363.8nm	Au 363.8nm	Au 532.0nm
I W/cm ²	64	6	6	6	6	32
Glass	2 min	15 s	2 min	1 min	10 s	1 min
Si	5 min	3 min	-	-	-	-
Quartz	3 min	6 min	10 min	4 min	-	-
stainless steel	5 min	2 min	-	-	-	-

for 532 nm laser induced deposition it was necessary to use a higher intensity than at 363.8 nm. The measured laser spot was 2.7 mm in diameter for the induction of NPs. For long exposure times, the metal deposition of NPs on the substrate appeared to be continuous. The sizes of all TPIs depended on the laser spot size, exposure time, and the Gaussian distribution of intensities for the lasers employed. To surpass the problem related Gaussian distribution of laser intensities of the laser irradiation, the spot size was expanded to 15 mm in diameter, and the laser power was increased to 1.2 W for 363.8 nm. Using these parameters, a TPI of 10 mm in diameter was obtained.

The minimum exposure times required for a desirable induction process were found to be substrate dependent. Table 2–1 shows the minimum exposure times for the induction of NPs on glass, quartz, stainless steel and silicon. Minimum exposure times were operationally defined as the time required for the deposition to be noticeable to the naked eye. Glass substrates had the lowest radiation exposure requirements to obtain continuous metal NPs deposition by induction in comparison to quartz for all metal NPs used at 363.8 nm laser inductions. The quartz substrates are transparent at this wavelength but glass substrates absorb the laser energy at this wavelength. This may indicate that heating of the surface due to laser incidence and absorption at the laser wavelength could be promoting the growth of nanostructures. Because the heat on a surface is proportional to the absorption coefficient and the laser intensity [13, 22] at constant laser power, the ET for NPs induction on glass is less than quartz. This is explained because for 532 nm

higher laser powers are necessary than for 363.8 nm because glass is transparent to this wavelength leading to less heat produced by the lower energy absorbed at 532 nm by glass. Fig. 2-2(k) and Fig. 2-2(l) show optical microscopy images of a linear interference pattern (LIP) of Ag on glass generated using setup 3. The laser parameters used for this induction were 12.7 kW/cm^2 of laser power at a wavelength of 532 nm, a lens of 100 cm focal length, and $\theta = 1.5^\circ$. The LIP generated was designed to produce a period of repetition of $23 \mu\text{m}$. This value agreed well with the period measured in Fig. 2-2(k) and Fig. 2-2(l) of $19 \pm 1 \mu\text{m}$. The induction was repeated two times more obtaining periods of $18 \pm 1 \mu\text{m}$ and $19 \pm 1 \mu\text{m}$. The value for the period obtained is sensitive to mechanical vibrations of the optical elements used by the laser induction setups, particularly when the setups are disassembled and reassembled. In order to achieve good reproducibility, a precision on micrometer-scale distances on the setups must be maintained. This applies to all of the setups used in the experiments. SEM images of this LIP were recorded for examining the wider consistency of the LIP period (see Fig. 2-2(m)) and the size and detailed nanostructure of the Ag-LIP formed (see Fig. 2-2(n)). The size of the nanostructures obtained ranged from 50 to 200 nm, but the SEM images obtained could not confirm fine details of the nanostructures due to limited resolution of the SEM equipment used. In Fig. 2-2(o) a 1 cent coin (penny) is included for size comparison purposes with the transferred pattern images of Ag and Au produced. The patterns have a size of 3 mm in this case and can be produced in much larger size by expanding the laser beam that generates the PI and TPI.

To obtain details of the NPs deposited on the substrate surfaces, Ag-NPs were detached from glass substrates by sonication in H_2O (see Fig. 2-3(a) and Fig. 2-3(b)). In the TEM images the size of NPs was between 2 to 100 nm. The size distribution was obtained from TEM images resulting in a mode of 9 nm and had a tail that extended to 100 nm. AFM topography images of TPIs of Ag-NPs on glass (2.6 W/cm^2 and 5 s of induction) are shown in Fig. 2-3(c) and Fig. 2-3(d). These images obtained at different sites of the TPI show that the nanostructure depths range from 0 to approximately 170 nm. Measurements of

the root-mean-square roughness (RMS-R), peak-to-valley roughness (PV-R) and average roughness (A-R) were determined for three different linear regions and area regions for the image shown in Fig. 2-3(c). The results are reported in Table 2-2. An A-R of 2 to 11 nm was determined in the analysis, the RMS-R was 3 to 17 nm and the PV-R was 11 to 171 nm, but the size distribution is wide. This is indicative of a non-normal distribution. This result is in agreement to the size distribution obtained for the TEM images and indicates that a random growth dominates part of the induced laser deposition process. The reproducibility of the depositions of NPs to form TIP and the thickness of NPs deposits were investigated using a profilometer (KLA-Tencor; model P-6, Milpitas, CA). Scans of TPI were acquired at a scan speed of 10 $\mu\text{m/s}$, sampling rate of 50 Hz and 1 mg of force. The thickness for 3 substrates (illustrated in Fig. 2-2(b)) of Ag-NPs at an ET of 120 s (1.7 W/cm^2 of 363.8 nm) was measured in duplicate on edge of the TPI and 1 substrate at exposure time of 60 s (same conditions and laser intensity). These are shown in Fig. 4-1(a). At the beginning of the scan the profilometer measured the thickness of the substrates well. However, subsequent dragging of NPs with little adhesion altered the results. This is shown by a circle in Fig. 4-1(a). The results obtained for all of the TPIs obtained from exposure times of 120 s (5 samples) are not present in the substrate of exposure time of 60 s, which is characterized by a smaller thickness of the sample because the lower exposure time to the laser action. The thickness or the amount of deposited material depends of the ET. This concept has been previously discussed in the literature [6, 20]. Average values for thickness and heights calculated for each measurement were obtained for the range shown in Fig 4-1(a). This range was selected from the analysis of the thickness of the substrate of exposure time of 60 s where there was not dragging of NPs caused by the profilometer probe. The variation coefficient was less than 12% for all cases and the average thickness for the substrate of ET of 120 s was 1.00 ± 0.07 μm and 0.63 ± 0.07 μm for the substrate at 60 s of induction. A variance analysis was done for the cases of ET of 120 s and the findings

Table 2-2: Roughness indication parameters for AFM images

	Length/ μm	Area/ μm^2	RMS-R/nm	PV-R/nm	A-R/nm
line 1	5.1	-	17	19	11
line 2	4.2	-	3	12	2
line 3	4.8	-	3	11	2
Region	-	26	11	171	8

were that there is no statistically significant difference between the means of the all the cases studied at the 95.0% confidence level.

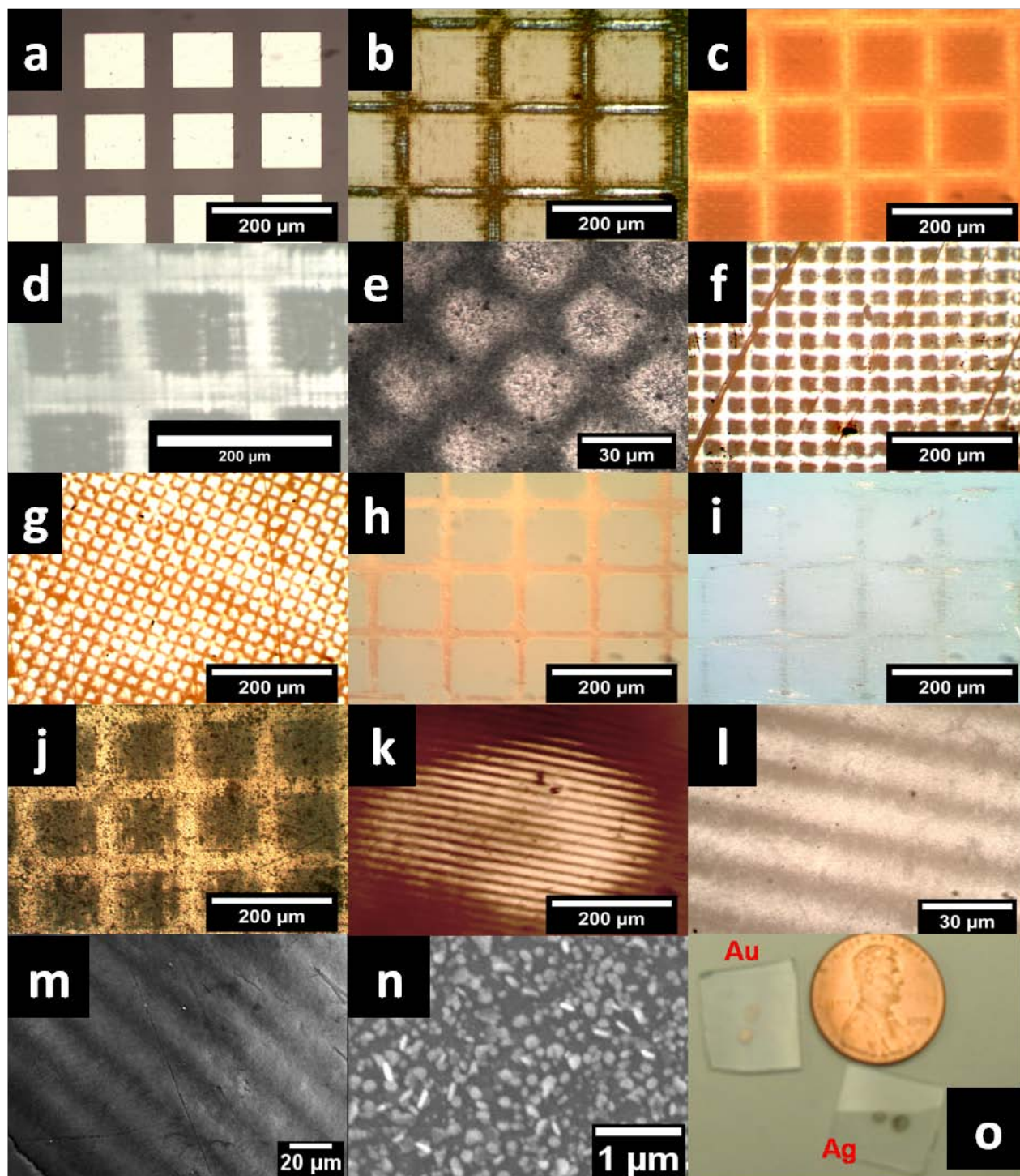


Figure 2-2: White light images obtained by optical microscopy. (a) Image of a beam splitter used as a grid: the white side is reflective to UV-Visible light while the dark side is transparent to UV-Visible light. (b) TPI made from Ag-NPs using optical setup 2, an intensity of 6.8 W/cm^2 at 363.8 nm and an ET of 60 s on glass as substrate. (c) TPI made from Pt-NPs using optical setup 1 and a 10 cm focal length lens ($d_o = 20 \text{ cm}$; $d_i = 20 \text{ cm}$) and an intensity of 1.7 W/cm^2 of 363.8

nm for 120 s on glass. (d) TPI made from Cu-NPs using optical setup 1 and a lens of 10 cm focal length ($d_o = 20$ cm; $d_i = 20$ cm) and an intensity of 1.7 W/cm² of 363.8 nm for 120 s on glass. (e) TPI fabricated using Ag-NPs and optical setup 1 using a lens of 2 cm focal length ($d_o = 70$ cm; $d_i \sim 2$ cm) at 2.3 kW/cm² of 532 nm for 10 s on glass. (f) TPI obtained from Ag-NPs using optical setup 1 and a 10 cm focal length lens ($d_o = 10$ cm; $d_i = 12$ cm) at 1.7 W/cm² of 363.8 nm at an ET of 120 s on glass (g) TPI prepared from depositing Ag-NPs using optical setup 1 using a lens of focal length 10 cm ($d_o = 10$ cm; $d_i = 12$ cm) at 1.7 W/cm² of 363.8 nm for ET of 120 s on glass. (h) TPI made from Au-NPs from optical setup 1 using a lens focal length 10 cm ($d_o = 20$ cm; $d_i = 20$ cm) at 6.7 W/cm² of 363.8 nm by ET of 300 s on Si. (i) TPI obtained from depositing Au-NPs with optical setup 1 using a lens focal length 10 cm ($d_o = 20$ cm; $d_i = 20$ cm) 6.7 W/cm² of 363.8 nm at an ET of 300 s on glass. (j) TPI of Au from Setup 1 using a lens focal length 10 cm ($d_o = 20$ cm; $d_i = 20$ cm) at 6.7 W/cm² of 363.8 nm at ET of 120 s on glass coated with 15 nm Cr. (k) Ag LIP obtained by using optical setup 3 using a 532-nm laser beam at 1.5° at 12.7 kW/cm² at an ET of 10 s on glass (l) 30- μ m scale marker image k. (m) SEM image of the same LIP. (m) 200-nm scale marker of the SEM image m. (o) Comparison of sizes of the transferred patterns with a penny.

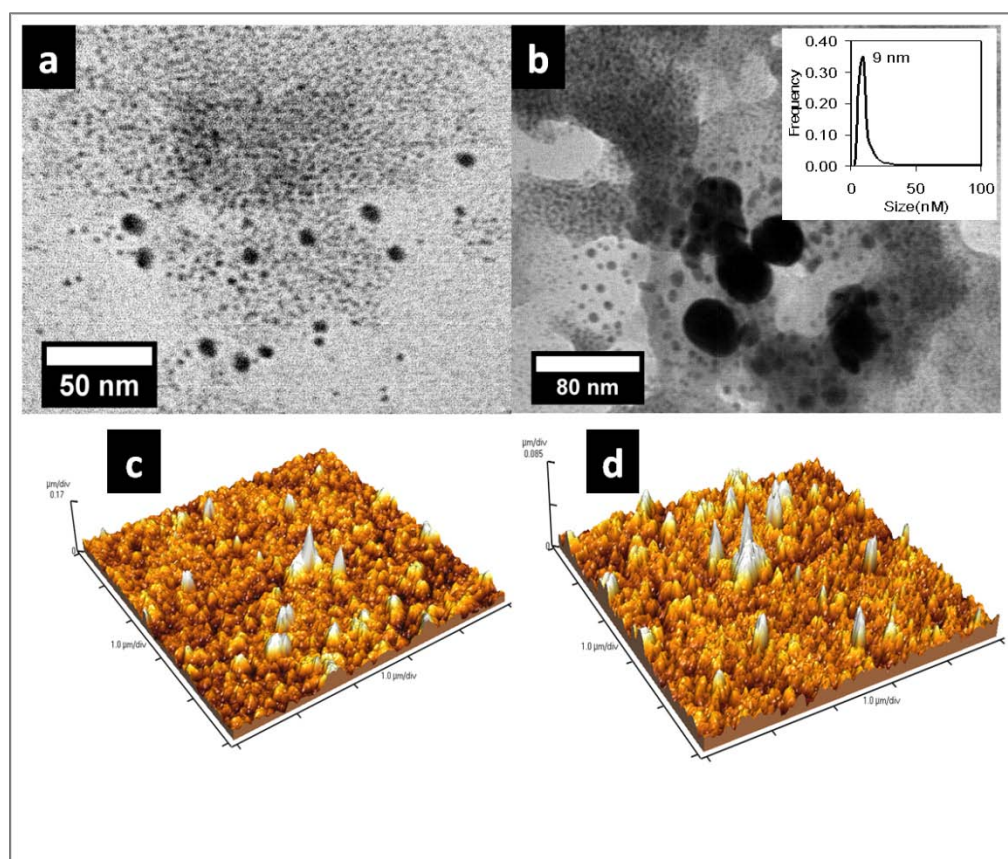


Figure 2-3: (a) and (b) TEM images for Ag-NPs detached from the glass substrate by sonication in H₂O (50 nm and 80 nm scale marker, respectively). (c) and (d): AFM images of the Ag TPI on glass in two different regions of the surface.

CHAPTER 3

KINETICS OF LASER-INDUCED GROWTH OF SILVER NANOPRISMS

3.1 Methodology and experimental setup

3.1.1 Materials

silver nitrate (AgNO_3 , 99.9995%-Ag, Puratrem) were purchased from Strem Chemicals. Sodium citrate dihydrate (99%) 4-nitro-benzenthionol (4-NBT) (99%), 4-amino-benzenthionol (4-ABT) (99%), sodium borohydride (98%), 4-nitro-thiobenzene (> 98%), Na_2S (> 98%) and 1,2-bis-(4-pyridyl)-ethane (BPE; 99%) were acquired from Sigma-Aldrich Chemical Co. (Milwaukee, WI); and 9H-purin-6-amine (adenine; 99.9%) was obtained from ICN Biomedicals (Aurora, OH). Laser systems used were a 532 nm frequency doubled solid state diode Nd:YAG laser (Verdi, 6W, Coherent Laser Group, Santa Clara, CA) and a continuous wave single line laser argon ion system model INNOVA 308 (Coherent Laser Group). The NPs and nanoprisms were characterized by a high resolution transmission electron microscope (HR-TEM), Zeiss model 922 operated at 200 kV and by an atomic force microscope (AFM) CP-II. The time-dependence UV-VIS-NIR spectra were recorded by a Varian Cary 5000 UV-Vis-NIR spectrometer.

3.1.2 Seed NPs form growth solution

The growth solution was prepared by basic method reported in the literature [23, 24]. A silver nitrate solution (100 mL, 0.1 mM) and trisodium citrate (0.5 mM) were stirred and 0.5 to 0.7 mL of NaBH_4 (10 mM) was added dropwise. A maximum of absorption in range of 398-401 nm was observed increasing in intensity with each droplet added. The addition

of NaBH_4 solution was stopped when the maximum absorption did not increase any further.

3.2 Experimental Setup

3.2.1 Kinetics of conversion to nanoprisms

In Fig. 3-1 a UV/VIS quartz spectroscopy cuvette with capacity of 50 L was illuminated with the laser beam at one its faces. An aliquot of 65 L of growth solution was placed in the cell and the growth induction was carried out. During the laser assisted growth, UV/VIS spectra were recorded every 10 min. The laser power was measured on the end of cuvette and used for calculating the laser beam intensity at the quartz window of the cell ($0.25 \text{ cm} \times 0.1 \text{ cm}$). Other inductions were realized in a 4 mL cuvette in order to obtain a larger volume of the nanoprisms synthesized.

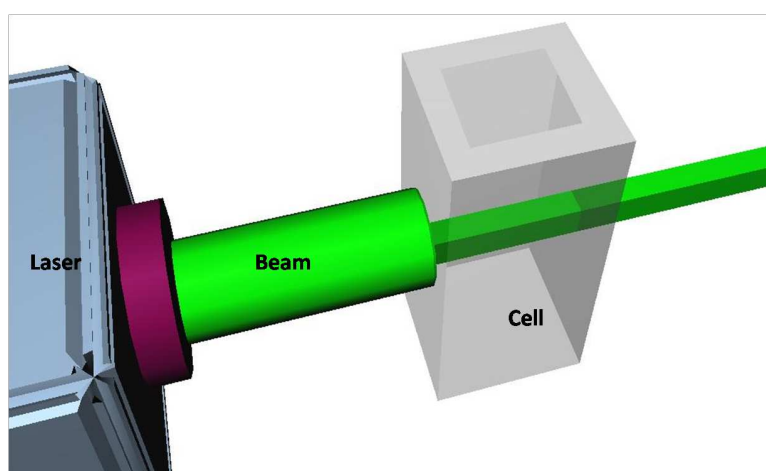


Figure 3-1: Setup for induction of conversion of nanospheres to nanoprisms

3.2.2 Raman Experiment

Raman measurements were conducted using a RM2000 Renishaw Raman microspectrometer equipped with a Leica microscope ($5\times$, $10\times$, $20\times$ and $50\times$ objectives). The spectra were collected in the Raman shift region of $200\text{-}3200 \text{ cm}^{-1}$ (0.5 cm^{-1} resolution), with an integration time of 10 s. SERS enhancement factors (EF) were calculated for analytes on substrates according to the equation 2.4

3.3 Results

3.3.1 Induction with different wavelengths

Fig. 3-2(a) shows the UV-VIS absorption spectrum for typical Ag seeds suspensions used in this investigation. Wavelengths for laser lines used for growth induction of Ag NPs are shown as vertical lines at the corresponding locations. A TEM image of these Ag NPs seeds is shown in Fig. 3-1(b). The mode of size of seed was 8.9 nm, calculated from an analysis of size distribution for the TEM images. The size distribution is shown in Fig. 3-2(c).

3.3.2 Growth induction using wavelengths shorter than 400 nm

NPs seeds were excited with laser wavelengths lower than 400 nm (max absorbance of Ag NPs seeds). Agglomerations of NPs were observed. This process is accompanied by an increase in the absorbance of the band of NPs colloidal suspensions at 400 nm but other processes leading to the destruction of the agglomerated NPs presented competition for larger scale nanostructures formation. Fig. 3-2(d) shows Ag NP agglomerated next to induction by 50 mW of the Ar⁺ UV laser line at 363.8 nm for 10 s. When the induction was conducted for longer times a decrease in absorbance was observed as shown in Fig. 3-3(a). Here the NPs were agglomerated and then precipitated. This was observed for other laser wavelengths in the UV (as for 244 nm shown in Fig. 3-3(b)). It was possible to generate nanostructures using UV laser lines from a solution of Ag⁺ ions in the presence of a reducing agent. Using 100 mW of a laser source at 363.8 nm on a 0.1 mM AgNO₃ solution a maximum absorbance was found at 400 nm at 400 s (Fig. 3-3(c)). If the induction was prolonged precipitation occurred. The shapes of the nanostructures were in the form of branches (flowers; see Fig3-3(d)). When the concentration of AgNO₃ was 1 mM a broadband was observed.

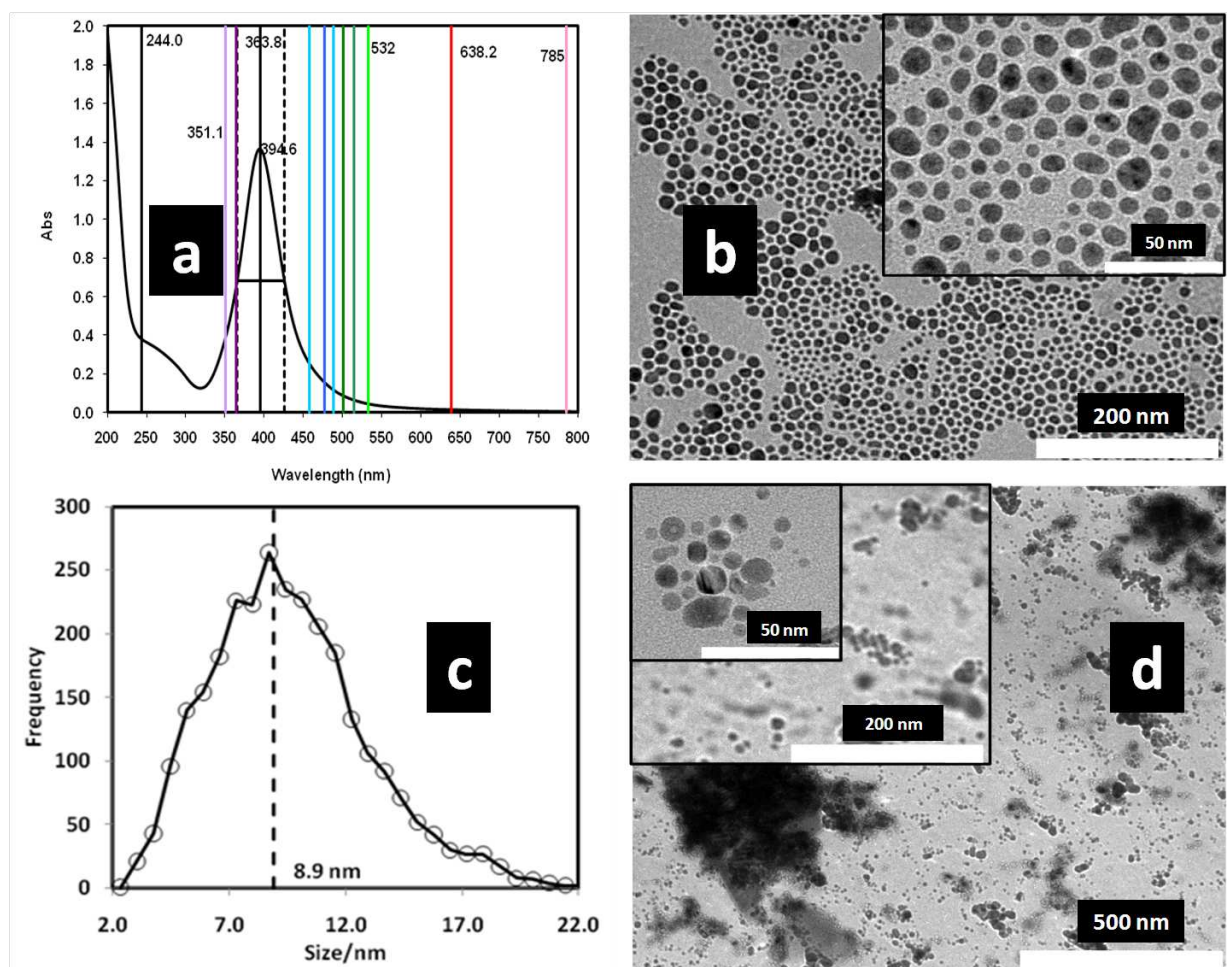


Figure 3-2: UV-Vis absorbance spectrum of Ag NPs seeds and their TEM images: a. spectrum of Ag NP seeds. Wavelengths location of laser lines used for the growth induction into nanoprisms are shown by vertical lines; b. TEM image of Ag seeds used for growth induction; c. size distribution of Ag NP seeds; d. TEM image of Ag seeds next to induction with 50 mW, 363.8 nm for 10 s

3.3.3 Induction of growth using wavelengths longer than 400 nm

When the growth induction was made with laser wavelengths longer than 400 nm a new VIS absorption band appeared at longer wavelength than 400 nm and nanoprisms were produced. The Ag NPs band at 400 nm increased quickly to a maximum in absorbance and then decreased slowly while the new band at longer wavelengths appeared (see Fig. 3-4(a) and Fig. 3-4(b)). A mechanism for the conversion of NP seeds is proposed with two principal steps. First, a fast agglomeration process of NPs seeds is induced and the rate constant for this process depends on the laser power. The first process was measured

Table 3–1: Rate constant for the agglomeration process for different laser powers and wavelengths

P/mW	I/Wcm ⁻²	k/s ⁻¹	k/s ⁻¹	k/s ⁻¹	k/s ⁻¹
		457 nm	488 nm	514 nm	633 nm
556	11.1			0.20(2) ¹	
166	3.31		0.12(2)		
133	2.65			0.060(4)	
41	0.83	0.059(4)	0.045(3)		
17	0.33	0.025(2)	0.0172(8)	0.014(3)	
13	0.26				0.0008(1)
7	0.13	0.012(1)	0.0050(5)	0.0037(2)	

using the fast increase of the band at 400 nm. Fig. 3–5(a) shows the dependence of the maximum absorbance at 400 nm with time for different laser powers for 514.5 nm irradiance. Fig. 3–5(b) shows the dependence of the maximum absorbance at 400 nm vs. time of the excitation wavelength: 457, 488, 514.5 and 633 nm (time scale for 633 nm is an order of magnitude higher). An exponential behavior was observed for all the cases studied and a strong dependence with laser power and excitation wavelength was found.

$$A_{\infty} - A = a [1 - \exp(-kt)] \quad (3.1)$$

The second step, the growth process for nanoprisms formation is controlled by the laser wavelength. This process was monitored using the appearance of the second VIS absorption band at longer wavelengths. An exponential behavior was also observed and a dependence on the laser power was confirmed too. The kinetics of the first process is exponential and a fitting for Equation 3.1 was made and the kinetics rate constant (k) was determined for different laser intensities and different excitation wavelengths (see Table 3–1).

$$k = \frac{dk}{dI} \quad (3.2)$$

Table 3-2: Quantum efficiency and coefficients of extinction for different wavelengths

λ/nm	dk/dI	A Ag NP Seed	ϵ	$\log(\epsilon)$
457	0.070(3)	0.156	1560	7.4
488	0.037(3)	0.063	629	6.4
514	0.0181(6)	0.032	323	5.8
633	0.0031(4)	0.006	58	4.1

The quantum efficiency is the relationship of the extinction coefficient for wavelength of the Ag NPs seed (see Table 3-2 and Fig. 3-5(d)). A linear dependence of k with laser power or laser intensity was found (see Fig. 3-5(c)). This is described by Equation 3.2, where dk/dI is the quantum efficiency

The second process or growth process was monitored using the new band that appeared at longer wavelength (see Fig. 3-6(a)). The behavior of the formation of this band is also exponential similar to Equation 6. This was done for 514.5 nm laser excitation at different power levels (see Fig. 3-6(b)). A fit was generated for the intensity vs. kinetics constant for the second process (k_2). The best fit is expressed as

$$k_2^2 = AI = (0.000132 \pm 0.000002)I \quad (3.3)$$

In order to find the quantum efficiency the first derivate obtained from Equation 3.3

$$\frac{dk_2}{dI} = \frac{1}{2} \left[\frac{A}{I} \right]^{\frac{1}{2}} \quad (3.4)$$

The process of conversion from NPs seeds to nanoprisms depends on the excitation of the plasmon of the NPs seeds. The excitation of the plasmon generates a polariton on the surface of NPs and it induces aggregation followed by fusion of the NPs to produce small crystals or in other words, nucleation. Next the small crystals grow and these have a favorite growth direction (see Fig. 3-7))

In these cases, the crystal growth is not driven by the diffusion of ions or molecules (see Appendix A) in the solution to the faces of the growing crystal. Instead, crystal growth

is generated by migration of Ag NPs seeds to the site at the crystal where the growth takes place and for this to happen Ag NPs seeds must be electronically excited. This is indication that the existence of plasmon on surface of Ag NPs seeds makes them more reactive and this is the driving force for nanoprisms growth. Fig. 3-7(a) to Fig. 3-7(d) are TEM images illustrating the crystal growth process from seeds to nanoprisms and its preferential direction of growth. This preferential direction of growth is responsible for the formation of nanoprisms, if the rates growths are equal in all direction, nanospheres would be formed instead of nanoprisms.

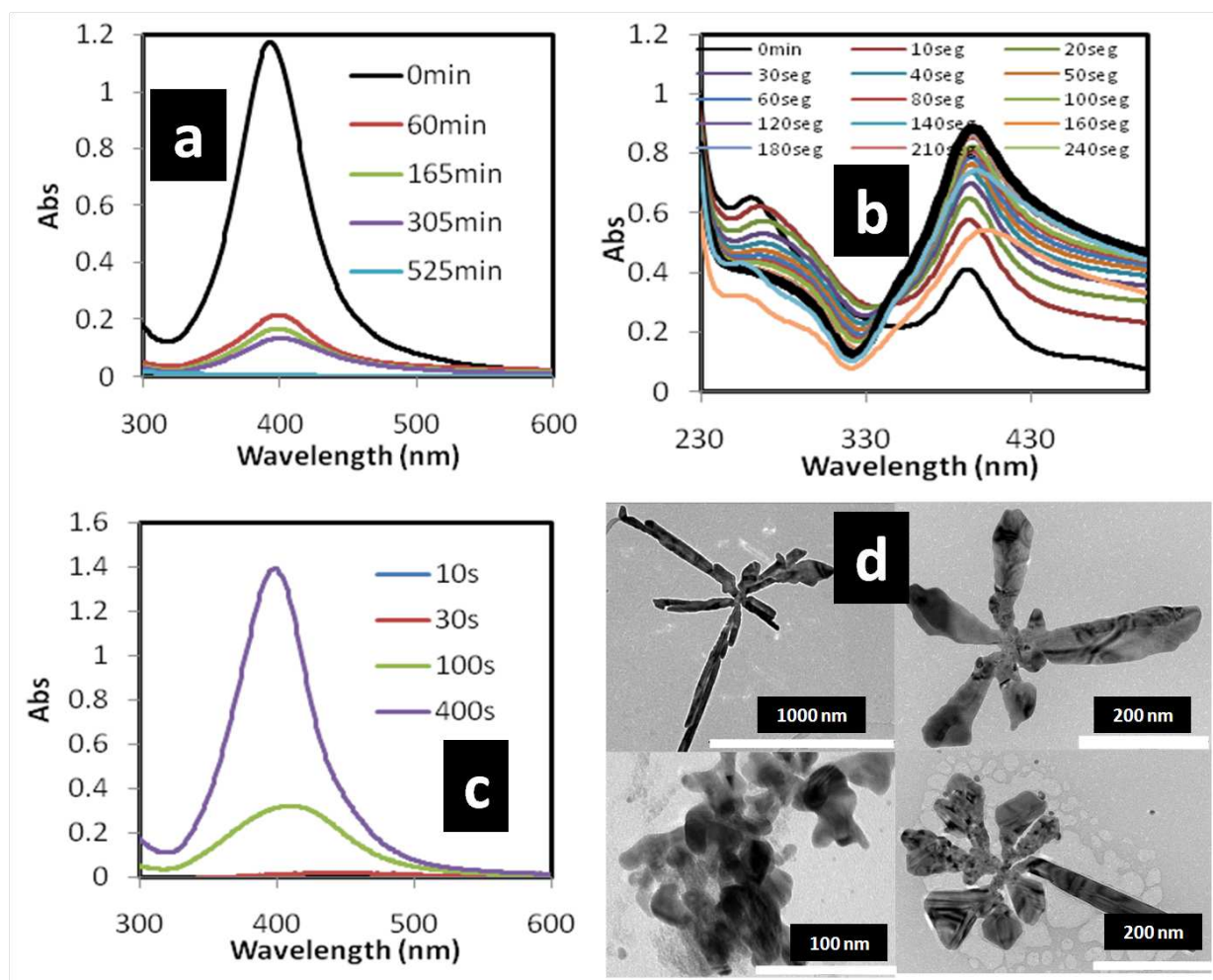


Figure 3-3: Laser assisted growth induction of NPs using UV light and TEM images of nanostructures produced: a. induction of Ag seed with 50 mW of 363.8 nm; b. induction of Ag seed with 24 mW of 244 nm; c. induction of growth for a solution 0.1 mM AgNO_3 plus 0.5 mM citrate; d. TEM image of nanostructures formed by laser induction of solution of Ag ions and in the presence of citrate

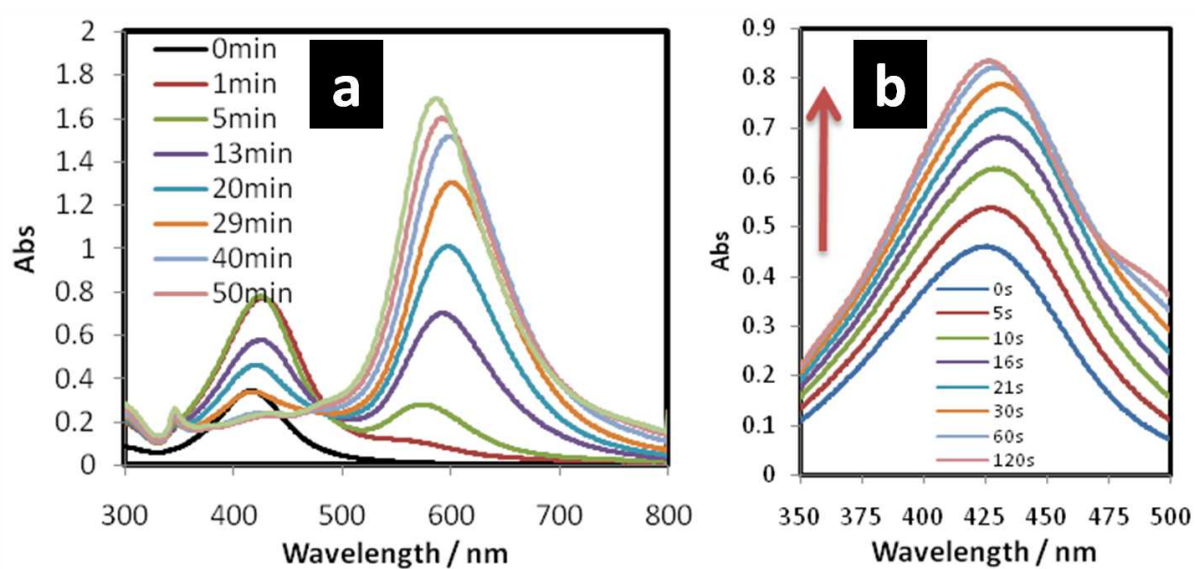


Figure 3-4: UV/VIS spectra at different induction times: a. using 674 mW of 514.5 nm. b. UV/VIS spectra in the region of band of absorbance for the NPs seeds at different induction times using 49 mW of 457 nm

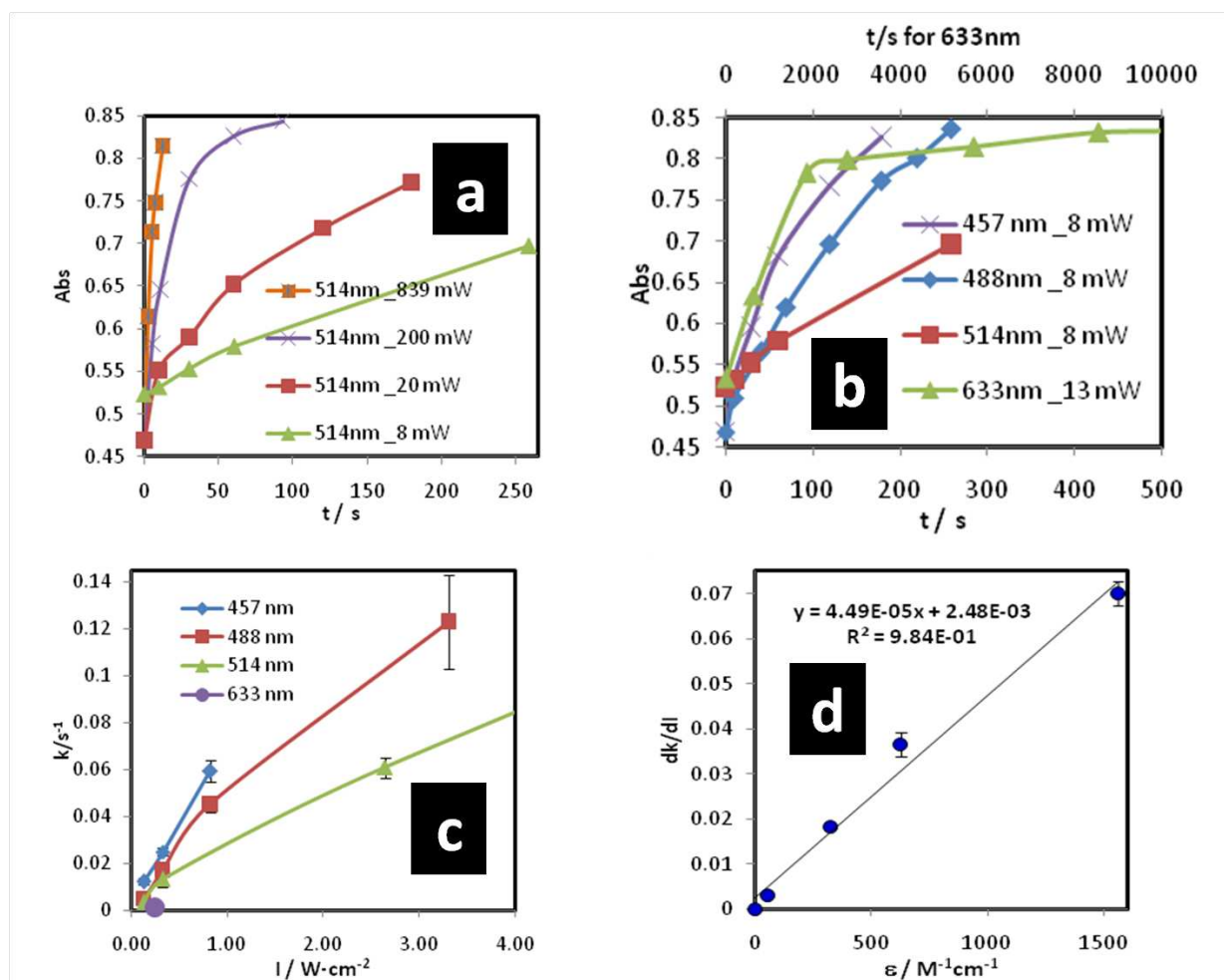


Figure 3-5: Kinetics of induction at different laser powers for the first process: a. absorbance of plasmon band at 400 nm vs. time for different 514.5 nm laser intensities; b. absorbance of plasmon band at 400 nm vs. time for different laser intensities and different wavelengths; c. kinetics rate constant vs. laser intensities for different laser wavelengths; d. quantum efficiency vs. extinction coefficient

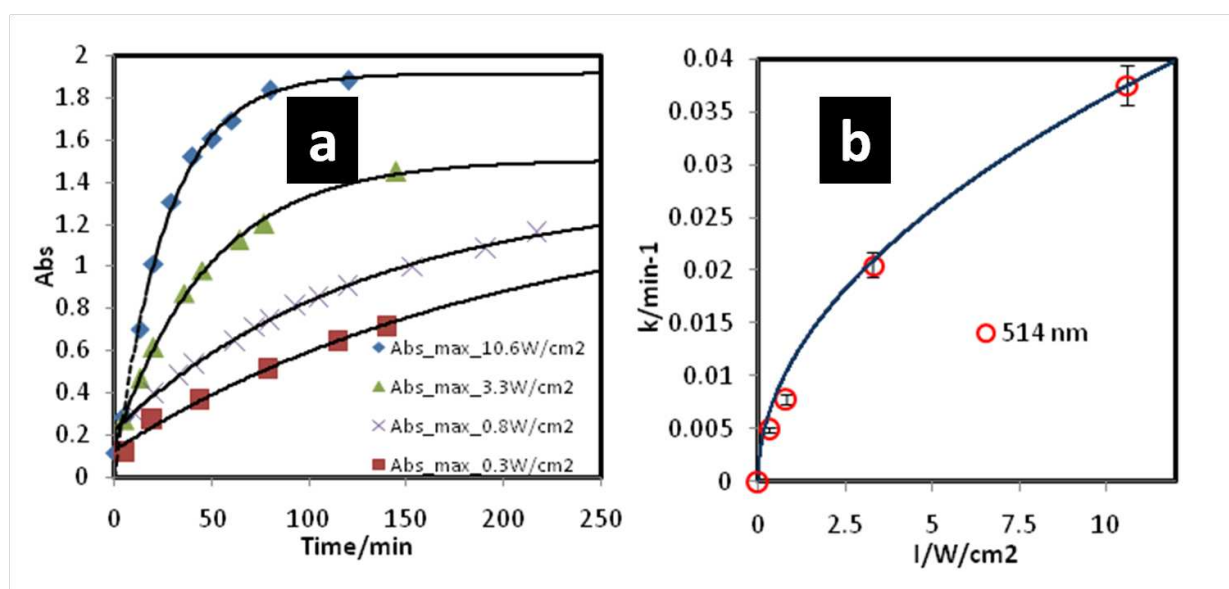


Figure 3-6: Kinetics of induction at different laser powers for the second process: a. maximum of absorbance vs. time for different intensities at 514.5 nm; b. kinetic rate constant vs. laser intensity for 514.5 nm

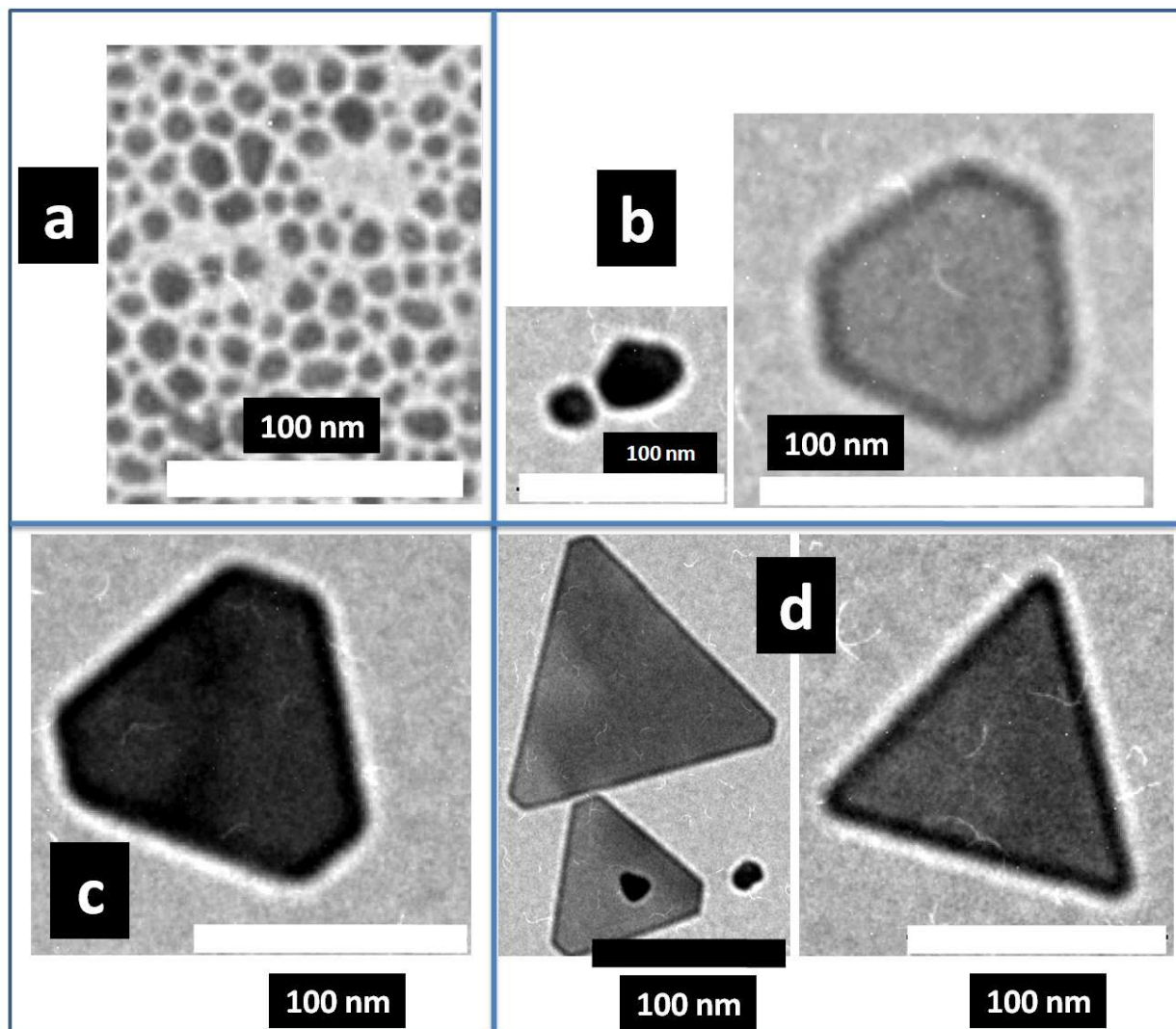


Figure 3-7: TEM image of crystallization process: a. Ag NPs seeds; b. nucleation and growth process; c. growth process on a preferential direction; d. formation of nanoprisms

CHAPTER 4

SURFACE ENHANCED RAMAN SCATTERING

4.1 SERS Activity for the micropattern

An application of the TPIs prepared by LIDS is in Surface Enhanced Raman Spectroscopy analysis (see Appendix A). The demonstration of SERS activity for Ag-NPs on glass TPIs is shown in Fig. 4-1(b). The background SERS spectrum for the TPI produced by deposition of Ag-NPs on glass generated at laser intensity of 1.7 W/cm^2 and ET of 60s is shown in Fig. 4-1(b) as a continuous gray curve. Raman spectrum of solid adenine is a dotted black line, and SERS spectrum of adenine for $4.3 \times 10^{-10} \text{ mol/cm}^2$ (1 L, 4.3×10^{-4} M adenine on 0.23 cm^2) is presented as a black continuous curve. This substrate had an enhancement factor EF 1.8×10^5 . The spectra were recorded at 532 nm laser excitation line and laser power of 0.5 mW and a 50 long working distance objective. Demonstration of SERS activity is shown in Fig. 4-1(c). The background Raman spectrum for Au-NPs on glass coated with 15 nm of Cr and generated at 6.7 W/cm^2 and an ET of 120 s appears as a gray continuous curve. SERS spectrum of probe molecule BPE at $8.1 \times 10^{-10} \text{ mol/cm}^2$ is shown as a black continuous line. The EF for this Au-NPs substrate was of 6.2×10^6 . This is slightly higher than the corresponding for adenine-Ag (Fig. 4-1(b)) but was recorded with a 785 nm of excitation line and laser power of 2 mW and objective of 50. Contamination of waste citrate is observed in the SERS spectrum of adenine but not in the SERS spectrum of BPE because the growth solution of synthesis of substrate of Au consisted of AuCl_4^- ions only. This is an advantage of SERS with Au-NPs based substrates to SERS with Ag-NPs based substrates. Another advantage is that Au-NPs based substrate is stable for activity SERS over several weeks (longer shelf life) but the Ag-NPs based substrate oxidizes readily.

In order to observe the SERS activity at different sites of a TPI two SERS line mappings were obtained for the pattern shown in Fig. 2-2(j). The line mappings were programmed so that the motorized platform would move the substrate in a linear form to expose the substrate to the exciting laser line through the middle of the left edge of the square box pattern towards the center of the box, exiting to the next box through the mid of the right edge into the next box, and so on. One of the line maps was obtained for the TPI fabricated from Au-NPs on glass with 15 nm of Cr coating and generated at 6.7 W/cm^2 and ET 120s. The Raman shift band of BPE at 1200 cm^{-1} was used to monitor the SERS line scans of the substrates. SERS spectra of $8.1 \times 10^{-10} \text{ mol/cm}^2$ BPE were recorded every $3 \mu\text{m}$ with an integration time of 2 s. Results are shown in Fig. 4-1(d). SERS activity is stronger in the areas where more Au-NPs are deposited (edges) than in the centers of the square grid.

4.2 SERS dependence on induction of nanoprism with different wavelengths

SERS activity of nanoprisms in aqueous suspensions was measured using BPE ($1 \times 10^{-4} \text{ M}$) as analyte and for $\lambda_{\text{max}} = 645 \text{ nm}$ plasmon of nanoprisms (synthesized from 532 nm laser induction, see Fig. 3-7(a)). SERS activity was compared to enhancements obtained by Ag nanospheres of similar characteristic dimension (average diameter). The concentration of Ag for both cases was 0.1 mM and the Raman spectra were recorded using 10 mW of 785 nm of excitation line for 10 s of integration time. Samples were transferred to the glass capillary tubes of 0.3 mm of diameter and the laser was focused using a $10\times$ objective. The maximum absorption of plasmon band of nanospheres was of 480 nm. The VIS absorbance levels of nanoprisms and nanospheres at 785 nm were 0.05 and 0.08, respectively. These values are similar for both shapes and can be used for comparison of SERS intensity. The nanoprisms had 2 times more activity than the nanospheres (see Fig. 4-2(a)) but in both cases it was necessary to add NaCl as agglomerating agent of the nanostructures to further promote SERS activity in BPE which was almost none for the nanoprisms if no NaCl was added. In the case of the SERS effect induced by nanoprisms, many bands were observed

in the region of 300 to 1000 cm^{-1} of BPE, which is fairly poor for nanospheres induced SERS. SERS activity was evaluated for 4-ABT (1×10^{-4} M) with different excitation lines and several types of nanoprisms. Nanoprisms synthesized by laser induction at 457 nm (indu-457nm) and 514 nm (indu-514nm) were used. Raman experiments were carried out at 532 nm and 785 nm. Maximum absorption of plasmon bands of nanoprisms were 486 nm and 569 nm, respectively.

SERS activity for 532 nm of excitation line was 5 times larger for nanoprisms prepared by laser induction at 457 nm (indu-457nm) than for nanoprisms synthesized by induction at 514.5 nm (indu-514 nm) as illustrated in Fig. 4-2(b). The maximum absorption of the plasmon band was located at 486 nm for indu-457nm. This value is located at a wavelength lower than the Raman excitation line used at 532 nm as opposed to indu-514nm for which maximum absorption of the plasmon band was located at 569 nm for which the Raman excitation line is at lower wavelengths (532 nm). This observation is an indication that it is better to excite the plasmon bands with Raman excitation lines $> \lambda_{\text{max}}$ of the absorption band. SERS activity was measured by excitation at 785 nm of for the same nanoprisms and the result was the opposite (see Fig. 4-2(c)). Increased SERS activity was found for indu-514nm. In this case the plasmon max is much closer to the laser excitation line and for this reason has stronger SERS activity. SERS activity at 785 nm is less than that excited by 532 nm because the plasmon band maximum is much closer to 532 nm (see Fig. 4-2(d)). As can be observed, there is a marked dependence of SERS activity and Raman excitation line of the plasmon band in nanoprisms because the monodispersity of the sample produces sharp absorption plasmonic bands that hinder plasmon excitation by wavelengths far from the maximum band absorbance (λ_{max}). However, the plasmon can be excited by tunnel effect when the wavelength of laser line is very far from plasmon band. Agglomeration of nanostructures for obtaining SERS activity in 4-ABT analyte was not necessary. This result is in marked contrast to SERS with BPE probe molecule. This is due

to the fact that 4-ABT is bound chemically by covalent bond formation with Ag nanostructures surfaces, contrary to BPE. This important results is based on the thiol group chemistry of 4-ABT which is very akin to the silver surface. In order to compare SERS activity between the various types of nanoprisms prepared and the excitation line the use of an agglomeration agent is not advisable because agglomeration tends to widen the plasmon absorption band, making nanoprism SERS activity similar. This obscures the observation of the dependence of SERS activity and excitation of the plasmon band components in nanoprisms. When an agglomerating agent was added to 4-ABT a slight intensity increase was observed but not as large as for the cases where the excitation of plasmon band had been effective without the agglomerating agent. The values obtained for the EF are indicative that SERS is highly augmented by a strong contribution of chemical mechanism due to covalent bond formation between the Ag nanoprisms and the SH end of the probe molecule.

4.3 SERS activity of nanoprisms on surface

In order to create SERS active substrates and improves its activity, nanoprisms were deposited on gold surface, to facilitate the adhesion of the nanoprisms to substrates, these were deposited on a gold surface pretreated with S^{2-} ions. The gold surface was dipped in a solution of S^{2-} ions (1×10^{-2} M). First, the nanoprisms solution was centrifuged and the supernatant water was replaced with fresh ultra high purity water. This process was repeated. Finally the solution was concentrated 10 times and 100 μ L of the resulting suspension was deposited on the gold surface. Fig. 4-3(a) and Fig. 4-3(b) show the images of nanoprisms deposited on gold surface with treated and not treated with S^{2-} , respectively. It is possible to observe a larger dispersion of the nanoprisms on the surface treated with S^{2-} . SERS activity was measured and compared for both surfaces. The SERS experiments were done using an objective of $5\times$ in order to provide for a wider surface coverage and spatial average. Laser line excitation at 785 nm was used. The laser beam at the sample plane was rectangular with dimensions: 200 μ m x 150 μ m. Many spectra on

the surface were recorded. The repeatability for the treated surface was 27% (coefficient of variation, CV) and 95% CV for the untreated substrate.

SERS activity was measured for 1 L of a solution of 4-NBT (1×10^{-4} M, 1×10^{-6} M, 1×10^{-8} M) deposited on an area 1 cm^2 . The spectra for 10 s of integration time are shown in Fig. 4-3(c). A comparison of spectra of nanoprisms and $1 \mu\text{L}$ of 1×10^{-4} M of 4-NBT on gold surface without nanoprisms is shown in Fig. 4-3(c) too. SERS signal was not observed for the nanoprisms on gold treated and a background is observed for the gold surface treated. In terms of mass detection, the amounts of 4-NBT detected ranged from 5 pg (5×10^{-12} g) to 0.5 fg (0.5×10^{-15} g). The enhancement factor (EF) was calculated based on the SERS measurements for the different concentrations and averaged. An average value for EF of 3×10^7 was determined for the nanoprisms and a plot of number of molecules vs. intensity of Raman shift band at 1570 cm^{-1} is shown in Fig. 4-3(c). A non linear behavior was observed. This represents a deviation from the values that can be calculated for the EF form Equation 2.4. A linear behavior between SERS activity and the number of molecules is required for Equation 2 to hold valid. However, in general, the EF values obtained for nanoprisms immobilized on gold substrates are higher than the corresponding EF values of nanoprisms in suspended in aqueous media for all the cases presented (i.e. for all solutions tested). A further improvement in the observed EF values can be attained by a tighter confinement of the nanoprisms on the substrate which in turn will augment the contribution from the electromagnetic mechanism to the SERS enhancements observed.

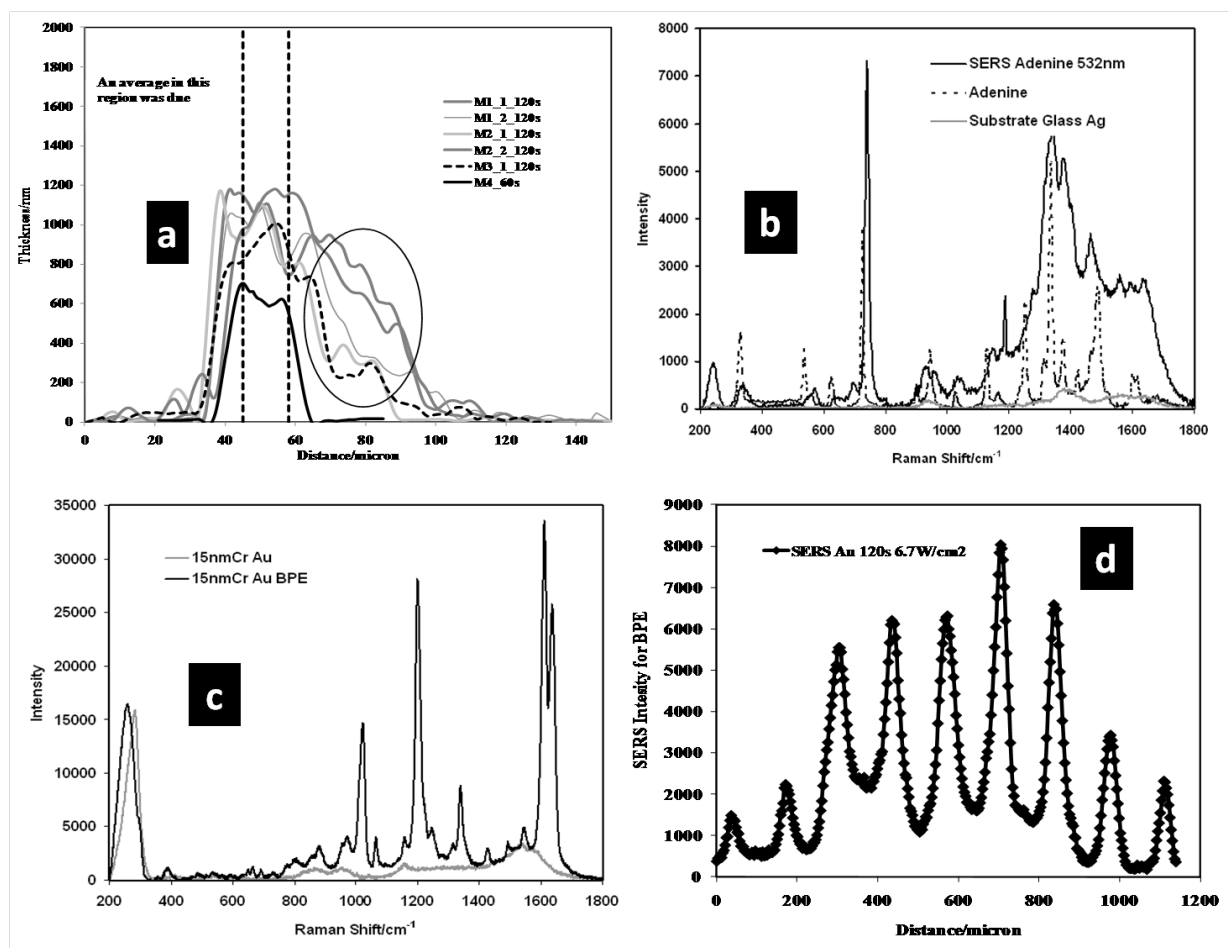


Figure 4-1: Depths of TPI, SERS spectra for TPI and lineal maps of SERS activity: (a) Depths of three TPI made from Ag-NPs at 120 s and their average value and one at 60 s of induction at laser intensity of 6.4 W/cm^2 . (b) SERS spectra of adenine deposited on Ag-NPs on glass prepared by a laser intensity of 1.7 W/cm^2 and ET of 60 s; background SERS spectra of same substrate and spectra Raman of solid adenine. (c) SERS spectra of BPE deposited on Au-NPs on glass with 15 nm Cr prepared by laser intensity of 6.7 W/cm^2 and ET of 120 s and background SERS spectrum of the substrate. (d) SERS line maps using BPE as SERS probe molecule on substrate prepared by depositing Au-NPs on glass coated with 15 nm Cr at a laser intensity of 6.7 W/cm^2 and ET of 120 s (black curve with diamonds) and 60 s (gray curve with squares). Gaussian fitting of intensity pattern included as reference (continuous thin curve)

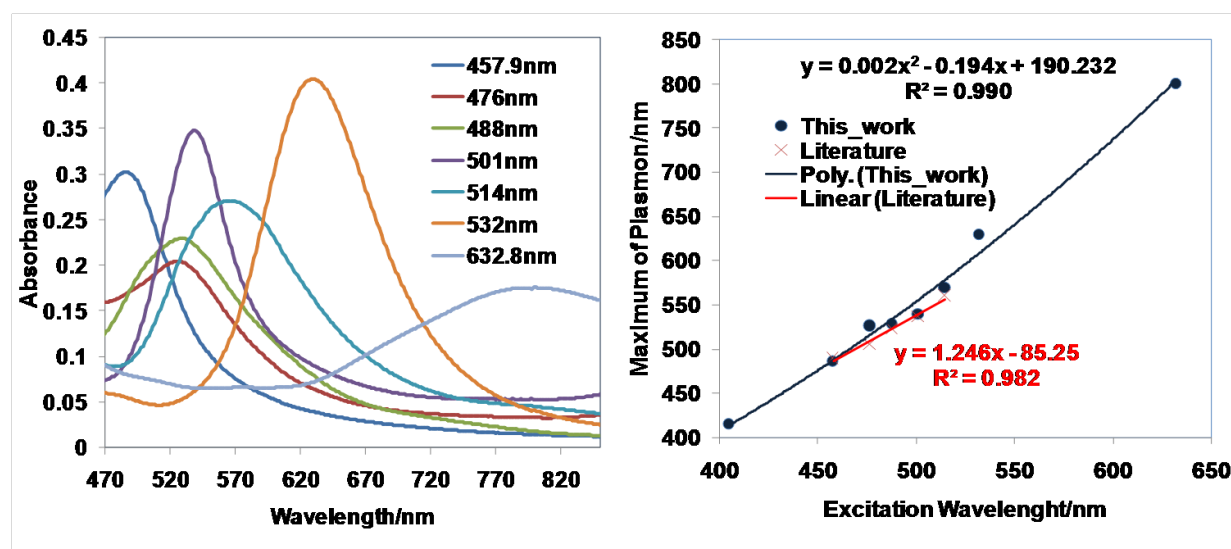


Figure 4-2: SERS activity of nanoprisms in solution: a. Comparison of SERS activity of nanoprisms and nanospheres using BPE at 785 nm excitation line; b. SERS activity of nanoprisms prepared at 457 nm and 514 nm using 4-ABT and Raman excited at 532 nm; c. SERS activity of nanoprisms prepared at 457 nm and 514 nm using 4-ABT and Raman excited at 785 nm; d. Comparison of enhancement factors (EF) of nanoprisms induced at 457 nm and 514 nm at two different excitation lines: 532 nm and 785 nm

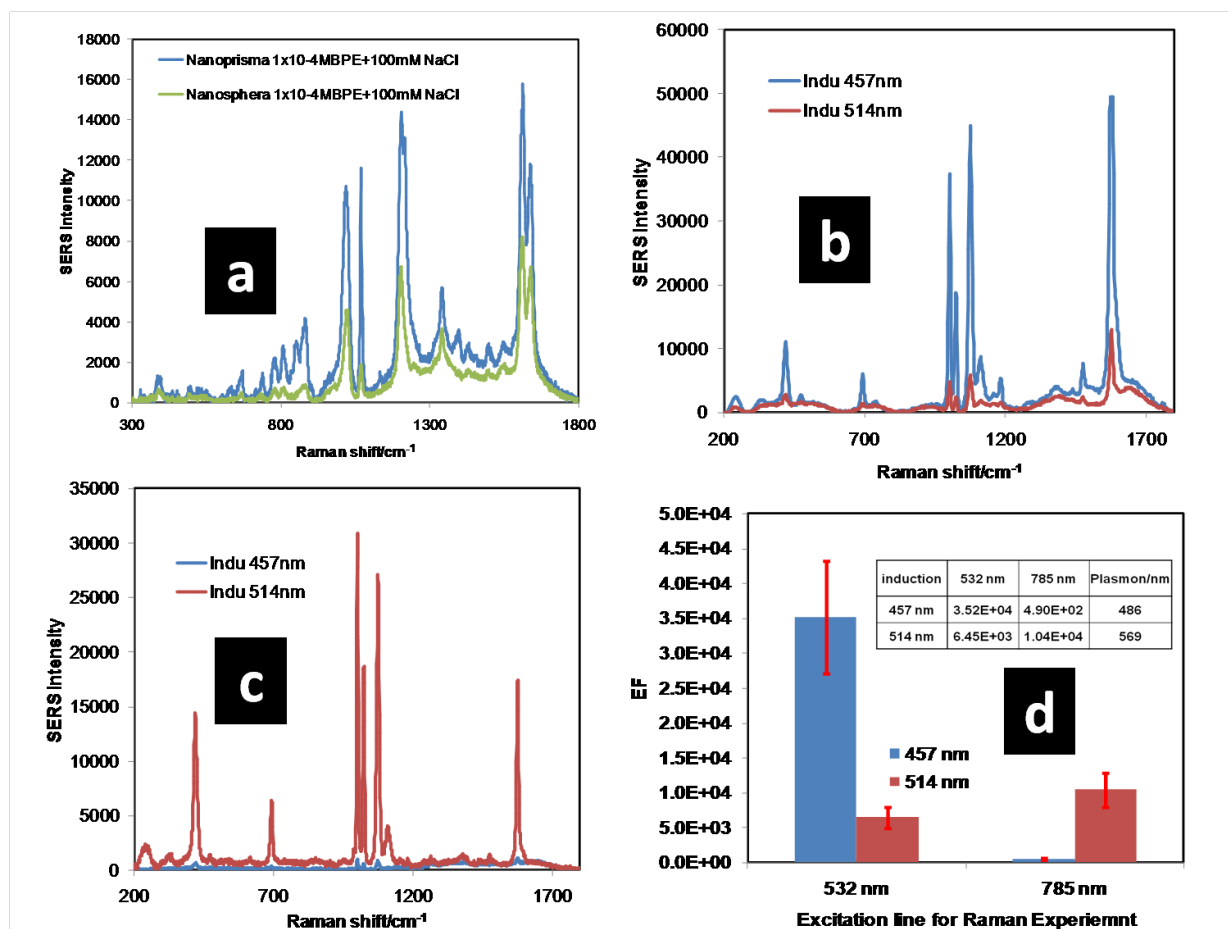


Figure 4-3: SERS activity of nanoprisms on Gold surface: a. Image of nanoprisms on gold substrate treated with S^{-2} . b. Image of nanoprisms on untreated gold substrate. c. SERS spectra of 4-NBT for: (I) 5 pg of 4-NBT; (II) 50 fg of 4-NBT; (III) 0.5 fg of 4-NBT; (IV) Raman spectrum of Au treated with S^{-2} , (V) Raman spectrum of 5 pg of 4-NBT on Au treated with S^{-2} . d. SERS intensity vs. number of molecules in the laser spot

CHAPTER 5

CONCLUSION

The deposition of NPs on different substrates by TPI was possible using laser-induced growth and laser-image formation. The size of the patterns of the PI (objects) was on the micrometers regime and the size of the TPI was on the millimeter scale. This size is limited by the wavelength of light (diffraction phenomena), the size of the object that acts as a PI to generate the image (TPI), and the optical setup employed. The lack of definition when the TPI is optically reduced is limited by the optical setup, because the process of deposition is random on the irradiated site and a penumbra effect induces a low quality growth on the surrounding area of the deposition. It is possible to generate a large area of a TPI with NPs in a short time and at low cost by using this methodology. TPIs in the form of different arrays and contrast can be used to confine NPs, acting as new substrates to deposit other NPs that avoid the materials build-up areas. The TPI fabricated this way represents an innovative and low-cost procedure for an optically approved, sensitive system and electric circuits applications, especially due to the evident easy pattern modifications that can be applied. The deposition of NPs for discontinuous or continuous metal coverage in the form of TPIs can be used as arrays to further deposition of solutions of NPs in the empty squares. This phenomenon of built-up area can be prevented when NPs in solution are deposited on the surface after the solvent is evaporated.

The growth and conversion of Ag nanostructures using lasers depends strongly on the excitation source wavelength. The rate at which this process occurs also depends on the laser wavelength. The kinetics for the two processes was measured and the dependence of kinetics rate constant with laser power was obtained. The quantum efficiency for the

process at various laser wavelengths was measured too. In the first process or process of agglomeration a dependence on the probability of excitation of the plasmon band of the initial NP (Ag seeds) with the rate was found. The rate of agglomeration depends on the plasmon excitation and this first process is necessary for the second process to occur and controls indirectly the second process (growth process). The crystallization of nanoprisms and the growth of crystal are produced by the NP excited by light and the size of crystal is controlled by the wavelength of the incident light. The growth begins by an agglomeration process The growth begins by an agglomeration process followed by fusion of the nanoparticles to produce small crystals and finally the growth of crystals. The first process is contradictory with the literature because a growth by rearrangement and formation of spherical NP is proposed. The second process follows according to the literature.

SERS activity was proven for Ag and Au NP micropattern substrates; and nanoprisms of Ag in solution and on Au surface. Enhanced Raman spectroscopy measurements for micropatter were carried out for SERS probe molecules adenine at 532 nm for Ag-NPs substrates and BPE at 785 nm for Au-NPs substrates. The SERS activity at different sites of a TPI is found, to measure the different SERS activities a line mappings were obtained for a micropattern. SERS activity is stronger in the areas where more Au-NPs are deposited (edges) than in the centers of the square grid. A Gaussian behavior is observed on deposited for SERS signal because the Gaussian distribution of laser beam intensities was transferred to the deposition. The calculated enhancement factors were 1.8×10^5 and 6.2×10^6 for adenine and BPE, respectively. This EF values are good and for this reason the substrates can be used for the detection of analytes.

For the nanoprisms SERS activity was measure for three different analyte, different nanoprisms and different excitation line. SERS activity was measure for nanoprisms in solution aqueous and on surface. The activity SERS for the nanoprisms is better when those are on surface with a EF of 3×10^7 for BPE. It possible have a considerable repeatability of SERS

Activity when gold surface is treated with S^{2-} ions. This may be due to the high affinity of silver and gold by the S^{2-} . When the gold surface is treated with S^{2-} a monolayer is generated and this is a link between nanoprisma silver and gold surface.

APPENDICES

APPENDIX A

BACKGROUND INFORMATION

A.1 Nature of Light

A dual theory provides explanation for all the properties of light. The dual theory explains how light propagates both as particle as well as waves. When light interacts with itself the wave theory is more appropriate and when light interacts with matter the particle theory works better in explaining the observed phenomena. If one wants to fully understand the process of interaction of matter and light one must have a quantum description of matter and of light. [25] Quantum Optics provides an explication of light and the interactions of light-light and light-matter. Light has two different properties: polarization and coherence. Light emitted from an incandescent lamp has not coherence or fixed polarization but light emitted by a laser can has different states of polarization and has good coherence. The polarization of light is one of simplest quantum mechanical systems. It is possible to consider which of the possible states of polarization of light as a quantum state of light [26].

A.2 Crystallization

Crystallization is the process when a substance passes of liquid or gas state to a highly ordered solid state which must consist of a crystal comprising of a rigid lattice of molecule, atoms or ions. The organizations of these particles in the lattices are characteristic of the substance. This organization influences the shape of the crystal. This is produced by the smooth surfaces or faces developed as a crystal grows and depends of the internal structure and the rate of growth of face of the crystal. This causes that rarely two crystals are identical. Crystal growth can be explained by two types of theories, the surface energy theory

and diffusion theory. In the surface energy theory, the shape that the crystal assumes is the minimum surface energy. The diffusion theory, matter is deposited on a crystal face at a rate proportional to the difference of concentration between the solution and the face of crystal [27].

A.3 Diffusion theory of crystallization

This theory assumes that crystallization is reverse to diffusion and therefore the rate is governed by the difference between concentration at the solid surface and in the bulk solution. The diffusion process or rate (dm/dt) on face of a growing crystal is equal to:

$$\frac{dm}{dt} = KmA(C - C^*) \quad (\text{A.1})$$

where m is the mass of solid deposited in time t ; A is surface area of the crystal; C is solute concentration in the solution; C^* is equilibrium saturation concentration; and Km is the coefficient of mass transfer [27].

A.4 Surface Enhanced Raman Scattering

Surface Enhanced Raman Scattering (SERS) is a surface spectroscopy technique. When molecules are adsorbed on a roughened metal surface the inelastic or Raman scattering phenomenon is enhanced. The mechanism of this phenomenon is not completely understood. There are two well-known mechanisms that have been proposed for explaining the nature of the Raman signal enhancement observed at or near roughened or discontinuous metallic substrates: the chemical mechanism and the electromagnetic mechanism. The chemical mechanism depends on the formation of a bond or a quasi-bond between the metal surface and the analyte and transference of charge is induced together with an increased polarization of the analyte. This increases the probability of Raman phenomenon as depends on how the bond in the molecule are polarized as a result of the molecular orientation on the substrate via the bond formation. Another explanation of this mechanism can be

given from the point of resonance or pre-resonance between the energy of the photons and the energy of the new levels electronic formed due to the new bond between metal surface and the analyte. This type of phenomenon increases the Raman scattering probability. In the electromagnetic mechanism proposed a gradient of the electric field at the roughened or sharply discontinuous metal surface is generated on the neighborhood of analyte bound to the surface. This induces a polarization of the analyte and in turn augments the scattered Raman signal intensity. The scale of roughness is in the nanometer regime for an effective SERS activity to take place.

REFERENCE LIST

- [1] R. Aroca. *Surface-Enhanced Vibrational Spectroscopy*. Wiley: Chichester England, first edition, 2006.
- [2] J. Turkevich.; P. C. Stevenson.; J. Hillier. A study of the nucleation and growth processes in the synthesis of colloidal gold. *Discuss. Faraday Soc*, 11:55, 1951.
- [3] Z. Peng.; B. Spliethoff.; B. Tesche.; T. Walther.; K. Kleinermanns. Laser-assisted synthesis of au-ag alloy nanoparticles in solution. *The Journal of Physical Chemistry B*, 110(6):2549–2554, 2006.
- [4] X. Zhang.; C. R. Yonzon.; M. A. Young.; D. A. Stuart.; R. P. V. Duyne. Surface-enhanced raman spectroscopy biosensors: Excitation spectroscopy for optimisation of substrates fabricated by nanosphere lithography. *IEE Proceedings: Nanobiotechnology*, 152(6):195–206, 2005.
- [5] H. Wang.; C. S. Levin.; N. J. Halas. Nanosphere arrays with controlled sub-10-nm gaps as surface-enhanced raman spectroscopy substrates. *Journal of the American Chemical Society*, 127(43):14992–14993, 2005.
- [6] E. J. Bjerneld.; F. Svedberg.; M. Kall. Laser-induced growth and deposition of noble-metal nanoparticles for surface-enhanced raman scattering. *Nano Letters*, 3(5):593–596, 2003.
- [7] X. Zheng.; W. Xu.; C. Corredor.; S. Xu.; J. An.; B. Zhao.; J. R. Lombardi. Laser-induced growth of monodisperse silver nanoparticles with tunable surface plasmon resonance properties and a wavelength self-limiting effect. *The Journal of Physical Chemistry C*, 111(41):14962–14967, 2007.
- [8] J. R. Meyer-Arendt. *Introduction to Classical and Modern Optics*. Prentice-Hall, Inc: New Jersey, fourth edition, 1995.

- [9] C. Daniel.; F. Mcklich.; Z. Liu. Periodical micro-nano-structuring of metallic surfaces by interfering laser beams. *Applied Surface Science*, 208-209(1):317–321, 2003.
- [10] A. Lasagni; M. D’Alessandria.; R. Giovanelli.; F. Mcklich. Advanced design of periodical architectures in bulk metals by means of laser interference metallurgy. *Applied Surface Science*, 254(4):930–936, 2007.
- [11] A. Lasagni.; C. Holzapfel.; F. Mcklich. Production of two-dimensional periodical structures by laser interference irradiation on bi-layered metallic thin films. *Applied Surface Science*, 253(3):1555–1560, 2006.
- [12] A. Lasagni.; C. Holzapfel.; T. Weirich.; F. Mcklich. Laser interference metallurgy: A new method for periodic surface microstructure design on multilayered metallic thin films. *Applied Surface Science*, 253(19):8070–8074, 2007.
- [13] A. Lasagni.; F. Mcklich. Structuring of metallic bi- and tri-nano-layer films by laser interference irradiation: Control of the structure depth. *Applied Surface Science*, 247(1-4):32–37, 2005.
- [14] A. Lasagni.; F. Mcklich. Study of the multilayer metallic films topography modified by laser interference irradiation. *Applied Surface Science*, 240(1-4):214–221, 2005.
- [15] H. M. Phillips.; D. L. Callahan.; R. Sauerbrey.; G. Szabo.; Z. Bor. Sub-100 nm lines produced by direct laser ablation in polyimide. *Applied Physics Letters*, 58(24):2761–2763, 1991.
- [16] H. Shin.; H. Lee.; J. Sung.; M. Lee. Parallel laser printing of nanoparticulate silver thin film patterns for electronics. *Applied Physics Letters*, 92(23), 2008.
- [17] V. Mikhailov.; G. A. Wurtz.; J. Elliott.; P. Bayvel.; A. V. Zayats. Dispersing light with surface plasmon polaritonic crystals. *Phys. Rev. Lett.*, 99(8):083901, Aug 2007.
- [18] L. Balan.; C. Turck.; O. Soppera.; L. C. Vidal.; D. J. Lougnot. Holographic recording with polymer nanocomposites containing silver nanoparticles photogenerated in situ by the interference pattern. *Chemistry of Materials*, 21(24):5711–5718, 2009.

- [19] R. Jin.; Y. Cao.; C. A. Mirkin.; K. L. Kelly.; G. C. Schatz.; J.G. Zheng. Photoinduced conversion of silver nanospheres to nanoprisms. *Science*, 294(5548):1901–1903, 2001.
- [20] E. J. Bjerneld.; K. V. G. K. Murty.; Juris Prikulis.; Mikael Kll. Laser-induced growth of ag nanoparticles from aqueous solutions. *Chemphyschem*, 3(1):116–119, 2002.
- [21] F. L. Pedrotti.; L. S. Pedrotti. *Introduction to Optics*. Prentice-Hall International, Inc: London, fourth edition, 1993.
- [22] A. Lasagni.; M. D’Alessandria.; R. Giovanelli.; F. Mcklich. Advanced design of periodical architectures in bulk metals by means of laser interference metallurgy. *Applied Surface Science*, 254(4):930–936, 2007.
- [23] Y. Sun.; B. Mayers.; Y. Xia. Transformation of silver nanospheres into nanobelts and triangular nanoplates through a thermal process. *Nano Letters*, 3(5):675–679, 2003.
- [24] M. Maillard.; H. Pinray.; B. Louis. Silver nanodisk growth by surface plasmon enhanced photoreduction of adsorbed [ag+]. *Nano Letters*, 3(11):1611–1615, 2003.
- [25] G. Grynberg.; A. Aspect.; C. Fabre. *Introduction to Quantum Optics: From the semi-classical Approach to Quantized light*. Cambridge University Press:Cambridge, first edition, 2010.
- [26] G. Baym. *Lectures on Quantum Mechanics*. The Benjamin/cummings Publishing Company: London, first edition, 1969.
- [27] W. J. Mullin. *Crystallization*. Planta Tree: London, first edition, 2001.